Chapter 7

The Magnetopause

Definition: The Magnetopause = Boundary between the magnetosphere and the shocked solar wind.

Problem: Solar wind plasma entry - Is the region where solar wind plasma enters not part of the magnetosphere?

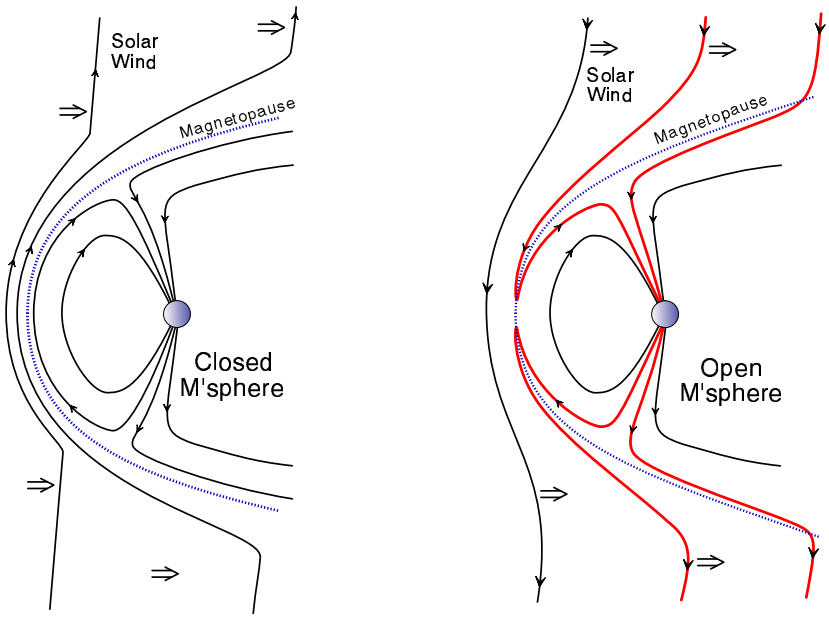

Figure 7.1: Sketch of closed and open magnetospheric configurations

More practical definition: The magnetopause is the region of highest current density and a mixture of particle of magnetospheric and magnetosheath origin.

This particularly refers to a local definition of the magnetopause as a

- tangential discontinuity in the absence of a magnetic field normal to the current layer

- rotational discontinuity in the presence of a magnetic field normal to a current layer

Magnetic Topology: 3 different types of magnetic connection for a field line

- Closed geomagnetic field lines (or magnetic flux) have both 'end' points in the Earth
- Open magnetic field lines have one footpoint on the Earth and connect with the other side to the solar wind
- IMF field lines are not connected to the Earth

Why is the magnetopause important?

- The MP controls the transport of mass, momentum, energy, and magnetic flux into the magnetosphere.
- The magnetic topology and the change of the magnetic topology are of major importance for the large scale transport (particles, momentum, energy) into the magnetosphere.

Can mass, momentum, energy be transmitted through a closed boundary into the magnetosphere?

- Mass: No, only very energetic test particles can enter the magnetosphere through non-adiabatic motion.
- Momentum and energy: Yes, via waves.

One can view the magnetopause as an active filter for linear and nonlinear perturbations in the solar wind and their action on the magnetosphere. To understand the role of the magnetopause for the magnetosphere one has to understand its structure and the processes which control the structure. Since the shocked solar wind and the magnetospheric plasma properties are different there is always free energy in the vicinity of the magnetopause and it is far from thermodynamic equilibrium. There are various instabilities which can and under the right conditions do operate at the magnetopause. These instabilities range from microscopic plasma instabilities which cause turbulence and local dissipation to macro instabilities such as the Kelvin-Helmholtz and the tearing mode.

A central problem of magnetospheric dynamics and space weather is the transport of mass momentum, and energy through the magnetopause boundary into the magnetosphere. For individual particles it is straightforward that they carry out a gyro motion around a magnetic field line combined with with various drifts caused by gradients and curvature in the magnetic field. However, these drifts are tangential to the magnetopause and do not provide any significant particle transport across the boundary. More formally ideal Ohm's law $\mathbf{E} + \mathbf{u} \times \mathbf{B} = 0$ implies the so-called frozen-in condition which states that the magnetic flux through any closed contour $\Phi_C = \int_C \mathbf{B} \cdot d\mathbf{s}$ moving with the plasma velocity $\mathbf{u}$ is constant in time. Equivalent, any two fluid elements are always connected by the same magnetic field line if they were connected at one time by this field line (defined by the direction of the magnetic field at any moment in time). In other words a magnetic field line can be identified by the motion of such fluid elements. This

can be extended to a more general form of Ohm's law when the bulk velocity $\mathbf{u}$ is replaced by the electron velocity $\mathbf{u}_e$ (compare discussion in 2.6).

Thus plasma on interplanetary field lines (without connection to the Earth) cannot penetrate into the magnetosphere without violating ideal MHD or Hall MHD (for a more general form of Ohm's law). Since the magnetospheric plasma is collisionless there is no large scale resistivity such that the violation of Ohm's law can only occur localized on very small scales. Note that momentum and energy can still be transferred into the magnetosphere through waves or viscous coupling. The most important processes for mass, momentum, or energy transfer into the magnetosphere are thought to be

- Magnetic reconnection
- Viscous interaction
- Pressure pulses and impulsive penetration

Examples and properties of these processes will be discussed in sections 7.3 and 7.4

7.1 Basic Properties and Observations

7.1.1 Boundary Normal Coordinates and Variance Analysis

It is common to use a local coordinate system for the magnetopause which is particularly helpful to identify typical properties in observations. This set of coordinates uses the capital letter L, M, and N to identify the coordinate directions with

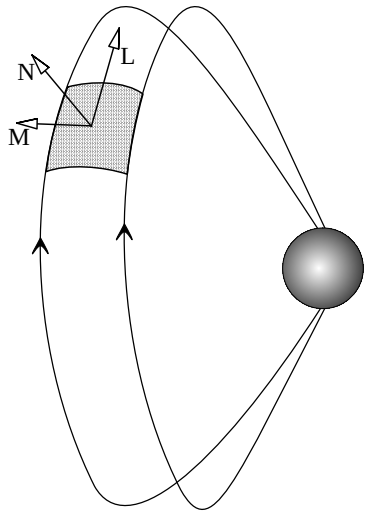

Figure 7.2: Sketch of boundary normal coordinates at the magnetopause.

- N being normal to the magnetopause surface

- L points into the local north direction (perpendicular to N) and
- M completes the coordinate system.

At the subsolar point these local coordinates can be compared to GSM coordinates (for a symmetric magnetopause). Here N corresponds to the x direction, L to the z direction, and M to the $-y$ direction.

However, how can one identify the magnetopause and provided it is well defined its orientation in terms of satellite observations? From a single satellite one obtains a time series of magnetic and electric field data and particle spectra which can be translated into the particle moments such as density, energy, and velocity. While the particle spectra give a general idea where the magnetopause might be, the transition from magnetosheath to magnetospheric populations can vary and does not provide direct information on the precise location and orientation of the MP.

A common diagnostic to identify the magnetopause is the variance analysis. This analysis assumes that the magnetopause boundary is a thin (one-dimensional) layer for which the temporal variation can be neglected during the time a satellite traverses this boundary. With these assumptions it follows from $\nabla \cdot \mathbf{B} = 0$ that the magnetic field in the normal direction is constant. Thus one needs identify a direction using the spacecraft data with an approximately constant magnetic field component.

Let us consider a fixed time interval with the magnetic field data given as series of measurements $B_\mu^{(i)}$ with $i \in [1, N]$ and μ indicates the magnetic field component (for instance x, y, or z in spacecraft coordinates).

The magnetic field variance matrix is now given by

$$M^B_{\mu\nu} = \frac{1}{N}\sum_{i=1}^{N} B_\mu^{(i)} B_\nu^{(i)} - \left[\frac{1}{N}\sum_{i=1}^{N} B_\mu^{(i)}\right]\left[\frac{1}{N}\sum_{i=1}^{N} B_\nu^{(i)}\right]$$

or in a more compact form

$$M^B_{\mu\nu} = \langle B_\mu B_\nu \rangle - \langle B_\mu \rangle \langle B_\nu \rangle$$

where $\langle\rangle$ indicates the average of the respective quantity. The determination of the Eigenvalues and Eigenvectors allows to determine the direction of minimum variance of the time series of vector measurements. The minimum variance direction is given by the Eigenvector with minimum Eigenvalue. On can easily convince oneself that this is a reasonable result. In this case $M^B_{\mu x} = 0$ and $M^B_{x\mu} = 0$ such that Eigenvectors with nonzero Eigenvalues are only in the the y, z plane. The Eigenvalue for the x direction is 0 as expected because there is no variation of the B_x component.

To overcome some of the difficulties with the magnetic field analysis, other quantities have been employed for similar analysis. In particular the mass flux $n\mathbf{u}$ should also be constant across a 1D stationary boundary. Commonly the magnetic field variance can be misleading if two direction with a rather small variation of the magnetic field exist. In these cases but also in general an electric field variance has been applied successfully. For the electric field (which is usually not the directly measured field but $-\mathbf{u} \times \mathbf{B}$) the maximum variance direction is the direction normal to the boundary. The reason for the the success

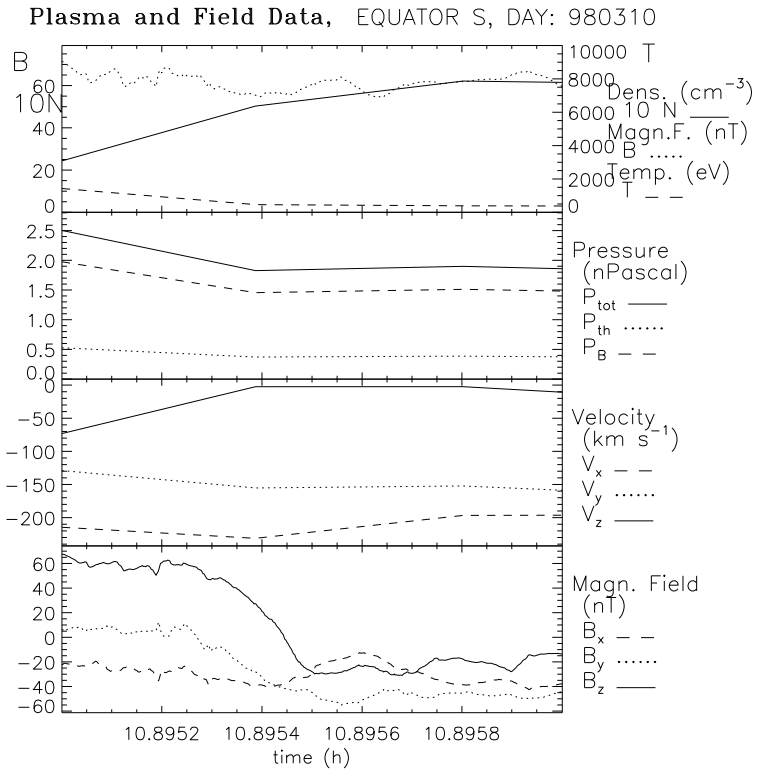

Figure 7.3: Equator S data of a magnetopause crossing on the dawnside flank of the magnetosphere.

of the maximum variance of the electric field is the frequently present large difference in the tangential plasma velocity across the magnetopause.

While the minimum variance of B is a rather standard diagnostic, realistic applications have a number of drawbacks. As mentioned the diagnostic requires time independence and a thin one-dimensional boundary. These conditions are never exactly satisfied. The real magnetosphere has a continuous spectrum of waves of different frequencies and wavelengths. These contaminate the data even if the actual boundary closely satisfies time independence and one-dimensionality.

Figure (7.3) shows data from the Equator S satellite of a magnetopause crossing on the dawnside (negative GSM y) flanks of the magnetosphere for a duration of 36 seconds. While it is rather obvious that the main rotation of the magnetic field occurs for the component. It is not at all clear whether there is a boundary and in what direction its normal would point.

Figure (7.4) shows the the magnetic field data (top) and the electric field data (bottom) from Figure (7.3) plotted as a hodogram: In a plane - for instance x and y - the corresponding vector components of the time series of the field (as measured by the spacecraft) are plotted. In this case the field is plotted as maximum versus intermediate (left) and as maximum versus minimum (right) directions. Values of the direction of the Eigenvector and the ratio of the Eigenvector are given in the Figure. The Eigenvectors in the maximum, intermediate and minimum direction are denoted as i, j, and k respectively. According to our prior discussion the normal of the boundary should be along the minimum variance direction $\mathbf{B}$ or the maximum variance direction of $\mathbf{E}$. The ratio of intermediate to minimum variance Eigenvalues for $\mathbf{B}$ is 4.5 which is reasonable but not particularly large. The ratio of maximum to intermediate direction for $\mathbf{E}$ is 108 which is very large and indicates an excellent maximum variance direction. Comparing

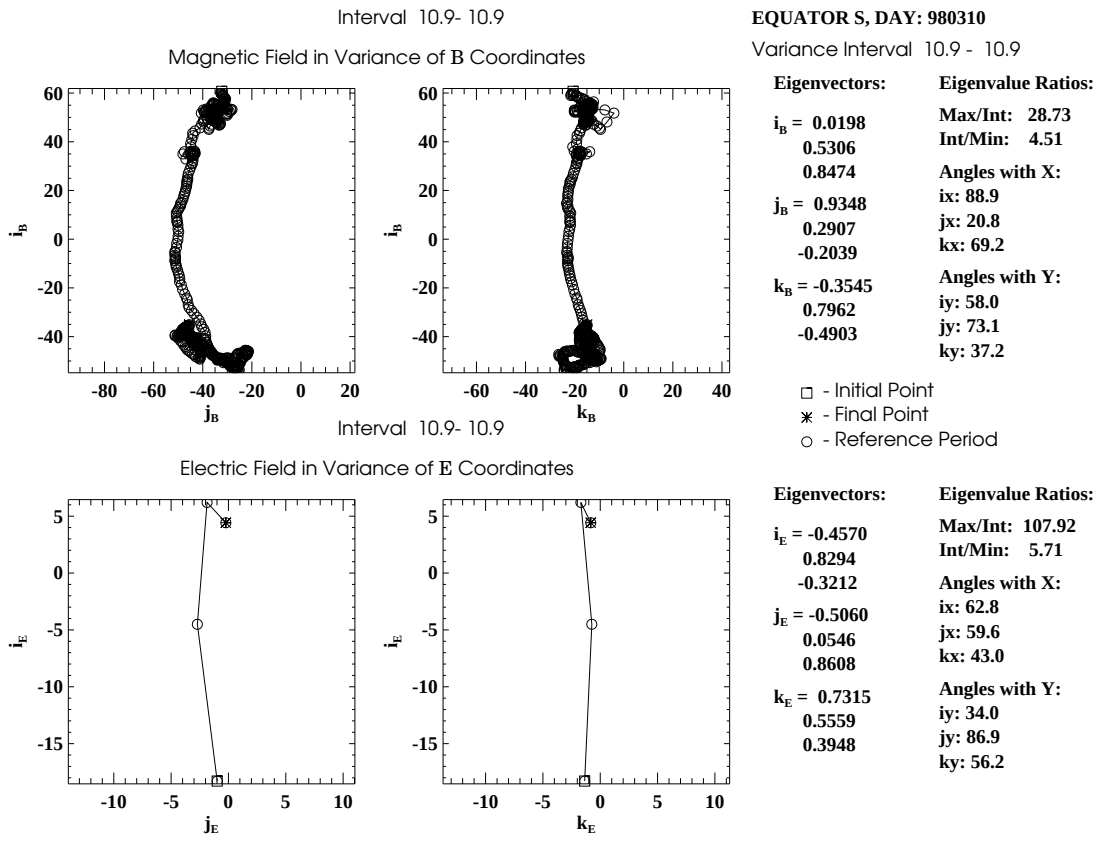

Figure 7.4: Hodogram of the magnetic field and the electric field in variance of B and E coordinates for data from the Equator S satellite.

the corresponding Eigenvector one finds that they are relatively close (the angle between $\mathbf{k}_B$ and $\mathbf{i}_E$ is only 11° but in view of the Eigenvalue ratios the Electric variance is likely more reliable. Note, however that there are only very few data points available for the electric field. This is common for satellite data because the electric field is determined from the measured $\mathbf{u} \times \mathbf{B}$ where the velocity is determined from the measured particle distribution function which in turn is sampled with the satellite spin period. Thus The temporal resolution of particle distributions and their moments is usually relatively low and with the spin period typically in the range of several seconds.

7.1.2 Magnetopause Shape

Solar wind dynamic pressure:

$$p_{dyn} = m_p n_{sw} u_{sw}^2$$

Here it is assumed that particles are ideally reflected from the magnetopause. Since the incident solar wind is only normal to the magnetopause surface at the subsolar point we need to consider the dynamic pressure which is normal to the magnetopause surface:

$$p_{dyn} = \kappa m_p n_{sw} \left(\mathbf{u}_{sw} \cdot \mathbf{n}_{mp}\right)^2$$

where we have introduced κ if the solar wind plasma is not ideally reflected or if the actual pressure acting on the magnetopause is modified otherwise. For instance the three-dimensional flow around the magnetopause tends to reduce the actual pressure.

On the magnetospheric side the dynamic pressure and usually also the thermal pressure can be neglected such that the corresponding pressure is given by the magnetic pressure

$$p_{msp} = \frac{B_{msp}^2}{2\mu_0}$$

Thus pressure balance in case of a tangential discontinuity reads

$$\kappa m_p n_{sw} u_{sw}^2 \cos^2\theta = \frac{B_{msp}^2}{2\mu_0} \tag{7.1}$$

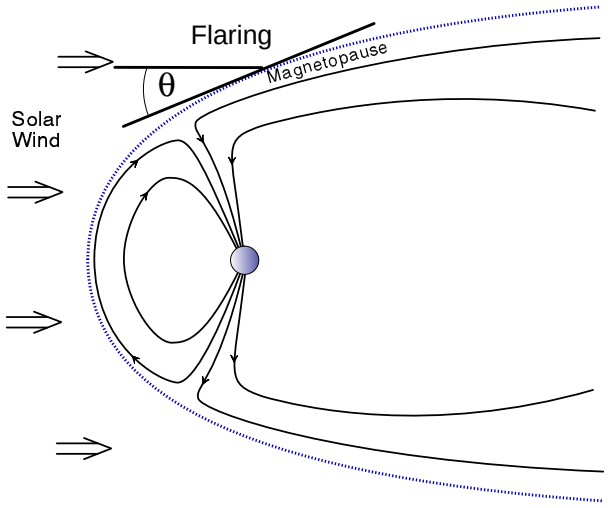

Figure 7.5: Illustration of magnetospheric flaring.

where θ is the angle between the magnetopause normal and the sunward direction. At the subsolar point we can approximately substitute the magnetic field with the dipole field

$$m_p n_{sw} u_{sw}^2 = \frac{K B_E^2}{2\mu_0 R_{mp}^6}$$

where K accounts for any deviation from the actual field from the dipole field and also absorbs κ. Thus the stand-off distance of the magnetopause is

$$R_{mp} = \left(\frac{K B_E^2}{2\mu_0 m_p n_{sw} u_{sw}^2}\right)^{1/6}$$

For $n = 5\,\mathrm{cm}^{-3}$, $u_{sw} = 400\,\mathrm{km}/s$, $B_E = 3 \cdot 10^4\,\mathrm{nT}$, and $K = 2$ we find $R_{mp} = 9.9\,\mathrm{R_E}$.

In regions where θ is close to 90° the dynamic solar wind pressure must be replaced with the thermal solar wind pressure $p_{th} = n_{sw} k_B T_{sw}$ such that the standoff distance approaches

$$R_{mp} = \left(\frac{K B_E^2}{2\mu_0 n_{sw} k_B T_{sw}} \right)^{1/6}$$

Equation (7.1) also provides information on the shape of the magnetosphere. The flaring angle is given by

$$\cos^2 \theta = \frac{B_{msp}^2}{2\mu_0 \kappa m_p n_{sw} u_{sw}^2}$$

However, one should keep in mind that the magnetic field strength on the magnetospheric side is not constant and it increases for a stronger compression, i.e., for larger dynamic pressure in the solar wind.

The asymptotic size of the magnetotail at large distance is determined by the magnetic flux in the tail. Assuming a circular cross section with radius R_T a magnetic flux of Φ in the northern lobe (semi circular cross section) the magnetic field strength in the tail is $B_T = 2\Phi/\pi R_T^2$. Since the flaring angle at large distance is 0 pressure balance becomes

$$n_{sw} k_B T_{sw} = \frac{2\Phi^2}{\mu_0 \pi^2 R_T^4}$$

which yields for

$$R_{mp} = \left(\frac{2\Phi^2}{\mu_0 \pi^2 n_{sw} k_B T_{sw}} \right)^{1/4}$$

One can estimate this magnetic flux by the flux in the near Earth tail (at 30 R_E distance with an average field of about 15 nT and a radius of about 20 R_E. A more sophisticated estimate has to include the amount of open flux and the amount of flux which crosses the equatorial plane and does not go out to the distant (>100 R_E) tail.

The magnetopause shape as discussed in this section uses a number of simplifications. Variations in the location can also be caused by the structure (open or closed) of the magnetopause and by processes in the magnetosphere which re-arrange magnetic flux.

7.1.3 Magnetopause Motion, Thickness, and Plasma Properties

The magnetopause moves quite rapidly with speeds of several 10 km/s in- and outward (viewed from the Earth). Thus a spacecraft traverses the MP in general not because of the SC velocity but because of this rapid magnetopause motion. The cause for this motion are variation in the upstream solar wind and changes in the magnetic field orientation which can lead to increasing or decreasing reconnection rates.

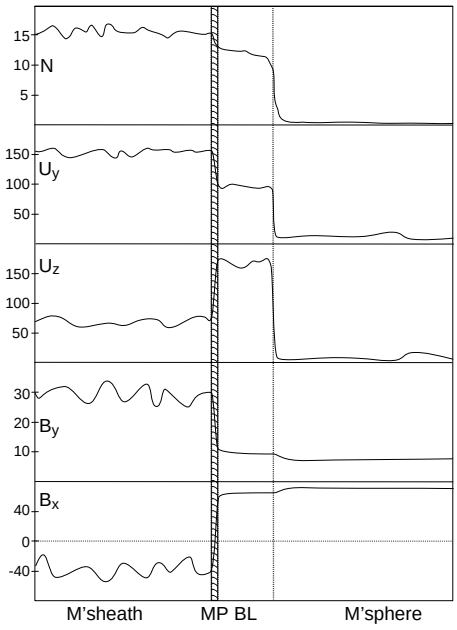

Figure 7.6: Illustration of a typical magnetopause observation

The magnetopause thickness is typically around 800 km but can vary between about 100 km and 2000 km. It is most easily identified in the subsolar dayside region. The structure is more turbulent and less obvious at the flanks and at high latitudes. The identification of the magnetopause as a current layer is particularly difficult for cases where the magnetospheric and the magnetosheath magnetic fields are largely aligned because the current density and field change is small.

A spacecraft entering the magnetosphere from the magnetosheath in the subsolar region (a region within 5 or 6 R_E of the subsolar point) would typically observe the following structure:

The plasma and the magnetic field in the magnetosheath are fairly disturbed. The SC encounter the magnetopause as a sudden large change of the magnetic field orientation (and magnitude) in the direction tangential to the magnetopause which is predominantly the y, z plane in GSM coordinates. The magnetic field turns predominantly into the northward z direction. At the magnetopause the density may decrease slightly. Typical for the region adjacent to the magnetopause is is a rotation (acceleration of the plasma velocity. This region of relatively fast flow and almost magnetosheath density is called the boundary layer and at low latitudes it is called the Low Latitude Boundary Layer (LLBL). The width of the LLBL is strongly varying and at times it may be entirely absent. However typical for this region is a width of several thousand km with increasing width for increasing distance from the subsolar region. At the dawn-dusk terminator the width is typically half an R_E.

7.2 Magnetopause Structure

7.2.1 Open or Closed Magnetopause Configuration

Locally there are various tests which can be applied to identify whether the magnetopause is open, i.e., whether there is a normal component of the magnetic field which connects the magnetospheric field to the solar wind, or whether it is closed, i.e. the normal magnetic field is 0.

First we could attempt to determine the normal magnetic field component through the variance analysis. Since the variance analysis provides an estimate for the normal direction the magnetic field along this direction would be the normal field component. However, noting that the normal direction is not determined with perfect accuracy and that the magnetic field component in the normal direction is expected to be small compared to the tangential field (the reasons for this will be discussed in the section on magnetic reconnection) any error in the normal direction would produce an apparent normal magnetic field. Thus the variance analysis cannot be used to predict the normal magnetic field.

If a normal magnetic field were present and the magnetopause is a thin boundary than there is only one MHD discontinuity (which is not a shock) that is consistent with a normal field. This solution is the rotational discontinuity. A rotational discontinuity has two properties which can be tested:

- DeHoffmann-Teller frame
- Nonlinear Alfvén wave

DeHoffmann-Teller frame

A DeHoffmann-Teller frame is a frame in which the convection electric field is 0 or

$$\mathrm{E} = -\mathbf{u} \times \mathbf{B} = 0$$

Consider a time interval with N measurements of the magnetic field and the velocity such the for an individual measurement i the electric field is

$$\mathrm{E}^{(i)} = -\mathbf{u}^{(i)} \times \mathbf{B}^{(i)} = 0$$

Using a transformation into a frame moving with the velocity $\mathbf{V}$ relative to the satellite the electric field becomes

$$\mathrm{E}'^{(i)} = -\left(\mathbf{u}^{(i)} - \mathbf{V}\right) \times \mathbf{B}^{(i)} = 0$$

To determine the transformation velocity one has to minimize the quantity

$$D(\mathbf{V}) = \frac{1}{N}\sum_{i=1}^{N}\left|\mathbf{E}'^{(i)}\right|^2 = \left|\left(\mathbf{u}^{(i)} - \mathbf{V}\right) \times \mathbf{B}^{(i)}\right|^2$$

The minimum of this expression is obtained by $\nabla_{\mathbf{V}} D(\mathbf{V}) = 0$ which yields

$$\underline{\underline{\mathbf{K}_0}} \mathbf{V}_{ht} = \left\langle \underline{\underline{\mathbf{K}^{(i)}}} \mathbf{u}^{(i)} \right\rangle$$

or

$$\mathbf{V}_{ht} = \underline{\underline{\mathbf{K}_0^{-1}}} \left\langle \underline{\underline{\mathbf{K}^{(i)}}} \mathbf{u}^{(i)} \right\rangle$$

where $\langle\rangle$ denotes the average over all data point and

$$\begin{aligned} K_{\mu\nu}^{(i)} &= B^{(i)\,2} \left(\delta_{\mu\nu} - \frac{B_\mu^{(i)} B_\nu^{(i)}}{B^{(i)\,2}} \right) \\ \underline{\underline{\mathbf{K}_0}} &= \left\langle \underline{\underline{\mathbf{K}^{(i)}}} \right\rangle \end{aligned}$$

Note that this minimization does not automatically imply the existence of a good deHoffmann-Teller frame. For a real plasma the average of the transformed electric field will never be exactly 0 but the quantity $D(\mathbf{V}_{ht})$ should be much smaller than for the originally measured velocities $D(0)$.

A test for the deHoffmann-Teller frame is plotted in Figure (7.15) (right). Here the actual electric field is plotted versus the dHT electric field $\mathbf{E}_{ht} = -\mathbf{V}_{ht} \times \mathbf{B}^{(i)}$. Ideally the data point should exactly line up along the diagonal (with slope 1). While this is not the case the data satisfies the relation very closely. This implies that the configuration is electrostatic, i.e., $\partial \mathbf{B}/\partial t = 0$. All steady state configurations belong to this group and in particular also a rotational discontinuity. The existence of a good dHT frame is a necessary but not a sufficient condition for a rotational discontinuity.

Walen Relation

We know that a rotational discontinuity implies a change of the velocity by

$$\Delta \mathbf{u} = \pm \Delta \mathbf{v}_A = \pm \Delta \frac{\mathbf{B}}{\sqrt{\mu_0 \rho}}$$

This relation is called the Walen relation. It is valid for linear and nonlinear Alfvén waves (the rotational discontinuity is a nonlinear Alfvén wave) and for switch-off slow shocks. With the transformation into the dHT frame the relation can also be written as

$$\mathbf{u}^{(i)} - \mathbf{V}_{ht} = \pm \mathbf{v}_A^{(i)} = \pm \frac{\mathbf{B}^{(i)}}{\sqrt{\mu_0 \rho^{(i)}}}$$

for each data point in the rotational discontinuity where either the $+$ or the $-$ sign applies. For the data of Figure (7.3) the plot in Figure (7.15) shows that the Walen relation is not satisfied. We therefore conclude that the boundary is not an open boundary (or the configuration is not a good one-dimensional current sheet).

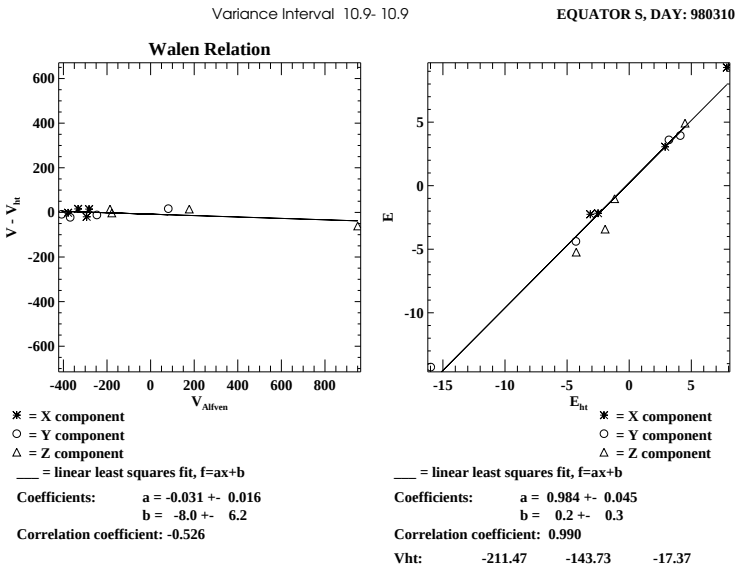

Figure 7.7: Tests of the deHoffmann-Teller frame and the Walen relation for the data set shown in Figure (7.3).

7.2.2 MP Currents

Large Scale Magnetopause Current

Figure 7.8 shows an overview of the MP currents using the assumptions that the currents are predominantly determined by the magnetospheric field adjacent to the magnetopause boundary. The magnetopause current is largely perpendicular to the geomagnetic field if the magnetic field outside the magnetosphere is small.

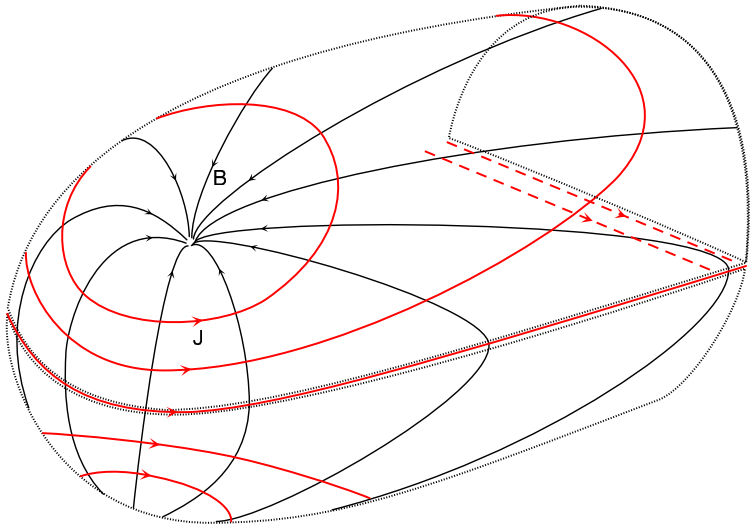

Figure 7.8: Sketch of the MP currents.

The currents on the dayside magnetopause close through the tail magnetopause. In the magnetotail the

northern and the southern lobes are separated by a cross-tail current layer. This current also closes over the tail magnetopause. A word of caution is needed with respect to this concept of current closure. Although $\nabla \cdot \mathbf{j} = 0$, a particular current line will in general not close in the simplistic way indicated in Figure 7.8. Currents do not originate in from some dipole as magnetic field lines and are generated locally. Thus any particular current line may be highly complicated and will in general not close in a simple way into itself. There is also no simple concept like a frozen-in condition applicable to current density. Currents are not bound to a particle plasma element.

Local Magnetopause Current

The local origin of the magnetopause current can be understood from the basic particle dynamics. Ions impinging on the magnetosphere have a larger gyro-radius than the electrons (Figure 7.9). Because of the larger gyroradius one expects them to determine the thickness of the magnetopause to approximately the ion gyro-radius. Ions move opposite to the electrons in this boundary layer. This generates a surface current which separates the the magnetosheath from the magnetosphere and change the magnetic field accordingly.

However, the typical magnetopause width is significantly larger than an ion gyro-radius (by about an order of magnitude). The reason for this discrepancy are the collective plasma effects which are not included in the above simplified model. To better understand the magnetopause (and other currents in the magnetosphere) we have to consider these collective effects for instance by using the fluid plasma equations. For the resulting drifts it is often important to consider gyrotropic pressure.

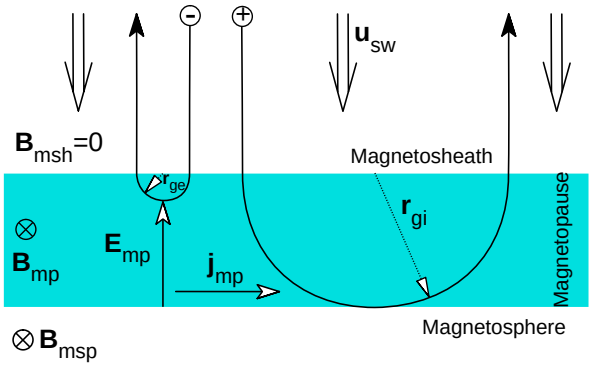

Figure 7.9: Illustration of particle dynamics at the magnetopause

Pressure Anisotropy

In many cases the pressure in the collisionless plasma of the magnetosphere is not isotropic. However the plasma is usually fairly gyrotropic meaning that it is well described by a parallel and perpendicular pressure. The reason for the gyrotropic pressure is the rapid gyro-motion which isotropizes the plasma motion efficiently in the plane perpendicular to the magnetic field. In this case the pressure tensor can be expressed as

$$\underline{\underline{\mathbf{p}}} = p_\perp \underline{\underline{1}} + (p_\parallel - p_\perp)\frac{\mathbf{BB}}{B^2}$$

Here as in the remainder of this subsection we have dropped an index s to indicate that the equations are valid for each particle species in a plasma. For both pressures the ideal gas equation is a good approximation

$$\begin{aligned} p_{\|} &= nk_B T_{\|} \\ p_{\perp} &= nk_B T_{\perp} \end{aligned}$$

If the adiabatic approximation is satisfied one can use the general definition of the adiabatic index

$$\gamma = (d+2)/d$$

with d being the degree of freedom. For the perpendicular motion we have $d = 2$ and for the parallel motion $d = 1$ such that the adiabatic equations of state are

$$\begin{aligned} p_{\|} &= p_{\|0} \left(\frac{n}{n_0}\right)^3 \\ p_{\perp} &= p_{\perp 0} \left(\frac{n}{n_0}\right)^2 \end{aligned}$$

However, the adiabatic equations do not consider the coupling between the parallel and perpendicular pressures. For instance the perpendicular pressure should increase as a particle distribution move into a region of larger magnetic field strength which is not the case for the adiabatic equations. Also the pressures are combined a measure for the internal energy such that the equations should satisfy energy conservation which is also not the case.

A better approximation can be found by considering the adiabatic invariants of single particle motion. Averaging the magnetic moment for a particle distribution function yields

$$\langle \mu \rangle = \frac{k_B T_{\perp}}{B} = \frac{p_{\perp}}{nB}$$

Since the average magnetic moment must be conserved (if the particle gyro-motion is faster than other temporal changes and the gyro radius is smaller than length scales of gradients in the plasma) the perpendicular adiabatic law is

$$\frac{d}{dt}\left(\frac{p_{\perp}}{nB}\right) = 0$$

The parallel adiabatic equation is more complicated and basically requires to consider energy conservations, i.e., it requires to integrate the collisionless Boltzmann equation for the parallel energy and for the perpendicular energy separately. The resulting equations can be combined to

$$p_{\perp}\frac{dp_{\|}}{dt} + 2p_{\|}\frac{dp_{\perp}}{dt} + 5p_{\perp}p_{\|}\nabla \cdot \mathbf{u} = 0 \tag{7.2}$$

With the continuity equation

$$\nabla \cdot \mathbf{u} = \frac{1}{n}\left(\frac{\partial n}{\partial t} + \mathbf{u} \cdot \nabla n\right) = \frac{1}{n}\frac{dn}{dt}$$

the pressure equation becomes

$$\frac{d}{dt}\left(\frac{p_{\|}p_{\perp}^2}{n^5}\right) = \frac{d}{dt}\left(\frac{p_{\|}B^2}{n^3}\right) = 0$$

With the ideal gas laws the equations of state can be re-written as

$$\begin{aligned} \frac{d}{dt}\left(\frac{T_{\perp}}{B}\right) &= 0 \\ \frac{d}{dt}\left(\frac{B^2 T_{\|}}{n^2}\right) &= 0 \end{aligned}$$

Thus a plasma which moves into a region of higher magnetic field strength will have an increasing perpendicular and a decreasing parallel temperature. This is for instance the case for the magnetosheath plasma as it gets closer to the dayside magnetopause with the result of an increasing temperature anisotropy.

Exercise: Show that the equation for the perpendicular kinetic energy is

$\frac{\partial}{\partial t}\left(\frac{1}{2}\rho u_{\perp}^2 + p_{\perp}\right) = -\nabla \cdot \left(\frac{1}{2}\rho u_{\perp}^2 + p_{\perp}\right)\mathbf{u} - \nabla \cdot p_{\perp}\mathbf{u}_{\perp} - \nabla \cdot \mathbf{L}_{\perp} - qn\mathbf{u}_{\perp} \cdot \mathbf{E}$

Exercise: Show that the equation for the parallel kinetic energy is

$\frac{\partial}{\partial t}\left(\frac{1}{2}\rho u_{\|}^2 + p_{\|}\right) = -\nabla \cdot \left(\frac{1}{2}\rho u_{\|}^2 + p_{\|}\right)\mathbf{u} - \nabla \cdot p_{\|}\mathbf{u}_{\|} - \nabla \cdot \mathbf{L}_{\|} - qn\mathbf{u}_{\|} \cdot \mathbf{E}$

Exercise: Show that by combining the above two equations and the momentum equations for parallel and perpendicular pressure one can derive equation 7.2.

Momentum Equation and and Fluid Particle Drifts

The fluid equation of motion for such a plasma is

$$\rho_s\left(\frac{\partial \mathbf{u}_s}{\partial t} + \mathbf{u}_s \cdot \nabla \mathbf{u}_s\right) = -\nabla p_{s\perp} - \nabla \cdot \left[(p_{s\|} - p_{s\perp})\frac{\mathbf{BB}}{B^2}\right] + q_s n(\mathbf{E} + \mathbf{u}_s \times \mathbf{B}) \tag{7.3}$$

Note that with a gyrotropic pressure the jump condition for the total pressure for plasma discontinuities becomes

$$p_{\perp} + \frac{B^2}{2\mu_0} = const$$

and the Walen relation for the normal velocity in rotational discontinuities becomes

$$u_n = \left[\left(\frac{B_n^2}{\mu_0\rho}\right)\left(1 - \frac{\mu_0(p_{\|} - p_{\perp})}{B^2}\right)\right]^{1/2}$$

For a stationary plasma with sufficiently small velocities (such that the $\mathbf{u}_s \cdot \nabla\mathbf{u}_s$ can be neglected) the force balance equation is

$$q_s n(\mathbf{E} + \mathbf{u}_s \times \mathbf{B}) = \nabla p_{s\perp} + \nabla \cdot \left[(p_{s\|} - p_{s\perp})\frac{\mathbf{BB}}{B^2}\right]$$

Taking the cross-product of this equation with $\mathbf{B}/B^2$ and dividing by $q_s n$ yields

$$\mathbf{u}_s = \frac{\mathbf{E}\times\mathbf{B}}{B^2} + \frac{1}{q_s n B^2}\mathbf{B}\times\nabla p_{s\perp} + \frac{1}{q_s n B^2}\mathbf{B}\times\nabla\cdot\left[(p_{s\|} - p_{s\perp})\frac{\mathbf{BB}}{B^2}\right] \tag{7.4}$$

which defines the fluid drifts in a stationary plasma configuration similar to the single particle drifts discussed earlier. The first term is the familiar $\mathbf{E}\times\mathbf{B}$ drift which has to be present as a result of the Lorentz transformation. The second and third terms are new and not present in this form in the single particle drifts. The new drifts arise due to the collective particle interactions.

The second term describes a particle drift perpendicular to the magnetic field and perpendicular to the gradient of the perpendicular pressure. This drift is called the diamagnetic drift. and is present if either a gradient in the density or a gradient in the temperature of the plasma exist (or both).

Let us consider a gradient in the plasma number density as illustrated in Figure . Particle gyrate in the magnetic field all in the same direction for the same charge. However, in the presence of a density gradient there are more particle in the direction of the gradient than in the opposite direction. Thus an observer at a fixed location would see more particle going in one direction (due to gyro-motion and due to the larger number of particle in the density gradient direction) then in the opposite direction. Thus at a given location a net bulk velocity arises due to the density gradient. Note that this does not require for the center of gyro-motion to move. Similarly a gradient in the temperature results in different gyroradii in the direction of the gradient with the same net result for the bulk motion.

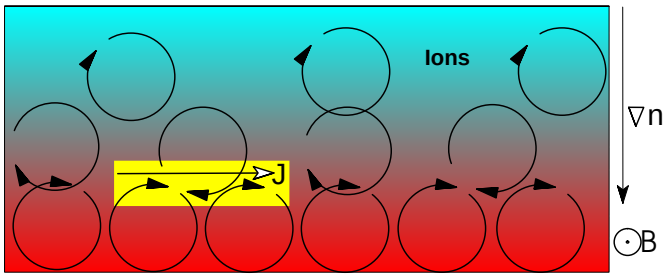

Figure 7.10: Illustration of the diamagnetic drift

Since the diamagnetic drift velocity

$$\mathbf{v}_{dia,s} = \frac{1}{q_s n B^2}\mathbf{B} \times \nabla p_{s\perp}$$

depends on the charge electrons and ions move in opposite directions giving rise to a diamagnetic current

$$j_{dia} = \mathbf{B} \times \nabla p_{\perp}$$

with $p_\perp = p_{e\perp} + p_{i\perp}$. If the plasma is isotropic the diamagnetic drift is the only plasma drift because $p_{s\|} = p_{s\perp}$.

For a non-isotropic plasma we can re-write the last term on the rhs of (7.4) using the radius of curvature definition as

$$\mathbf{v}_{dia,s} = \frac{p_{s\|} - p_{s\perp}}{q_s n B^2 R_c}\mathbf{B} \times \mathbf{n}$$

where $\mathbf{n}$ is the outer normal of the field line curvature and R_c is the radius of curvature. Thus this drift exists only for curved magnetic fields similar to the single particle curvature drift but it depends on parallel and perpendicular pressure and it can be positive or negative depending on the ratio of these pressures. The corresponding current density is given by

$$\mathbf{j}_{dia} = \frac{p_\| - p_\perp}{B^2 R_c}\mathbf{B} \times \mathbf{n}$$

where $p_\| = p_{e\|} + p_{i\|}$.

Applications of these drifts to the magnetopause are obvious If the magnetic field on the magnetosheath side is weak then there has to be a pressure gradient in order to maintain an approximate equilibrium situation. The perpendicular pressure gradient drives a diamagnetic current which in turn accounts self-consistently for the increase in magnetic field strength.

It should, however, be mentioned that the magnetic field in the magnetosheath is frequently not negligible. In such cases the pressure gradient is usually small such that the diamagnetic currents are small. In these cases the current is mostly field-aligned.

Exercise: Show that a magnetic field rotation in the absence of a pressure gradient (i.e., equal magnitude magnetic fields on the two sides of the magnetopause) implies the the magnetopause current is field-aligned.

Polarization Drifts

Thus far we have considered a stationary configuration. If there are slow changes in the configuration we can compute the additional drifts by including the inertia term in the equation for the electric field

$$q_s n(\mathbf{E} + \mathbf{u}_s \times \mathbf{B}) = \nabla p_{s\perp} + \nabla \cdot \left[(p_{s\parallel} - p_{s\perp}) \frac{\mathbf{BB}}{B^2} \right] + \rho_s \frac{\partial \mathbf{u}_s}{\partial t}$$

and by taking the cross-product with $\mathbf{B}/B^2$ and dividing by $q_s n$ obtain the additional term

$$\mathbf{v}_s = \frac{m_s}{q_s B^2} \mathbf{B} \times \frac{\partial \mathbf{u}_s}{\partial t}$$

where we can substitute

$$\frac{\partial \mathbf{u}_s}{\partial t} = \frac{\partial}{\partial t} \left\{ \frac{\mathbf{E} \times \mathbf{B}}{B^2} + \frac{1}{q_s n B^2} \mathbf{B} \times \nabla p_{s\perp} + \frac{1}{q_s n B^2} \mathbf{B} \times \nabla \cdot \left[(p_{s\parallel} - p_{s\perp}) \frac{\mathbf{BB}}{B^2} \right] \right\}$$

For the first term this results in the guiding center polarization drift

$$\mathbf{v}_{p,s} = \frac{m_s}{q_s B^2} \frac{d\mathbf{E}}{dt}$$

known from the single particle drifts. The second term yields a new polarization drift which in the case of constant magnetic field and temperature results in

$$\mathbf{v}_{pn,s} = \frac{m_s k_B T_s}{q_s^2 B^2} \nabla_\perp \frac{d \ln n}{dt}$$

Finally from generalized Ohm's law one obtains a drift similar to the ones above from the current inertia term:

$$\mathbf{v}_{pc,s} = \frac{m_e}{n e_s^2 B^2} \mathbf{B} \times \frac{\partial \mathbf{j}}{\partial t}$$

This drift is a motion of the bulk of the entire plasma such that it does not cause any current.

7.3 Magnetic reconnection

During periods of southward IMF magnetic reconnection connects closed geomagnetic field with interplanetary magnetic field generating newly opened magnetic flux (Figure 7.1). Along the newly opened field particles can freely enter and leave the magnetosphere. The newly opened field is swept with the solar wind along the magnetosphere and magnetic flux accumulates at the tail boundary. The accumulation of magnetic flux in the magnetotail lopes increases the size of the tail magnetosphere and magnetic energy is stored in the lobes of the magnetotail. Thus reconnection at the dayside magnetopause is important for the energy budget of the entire magnetosphere. The subsequent processes in the magnetotail will be addresses in the section on the magnetotail.

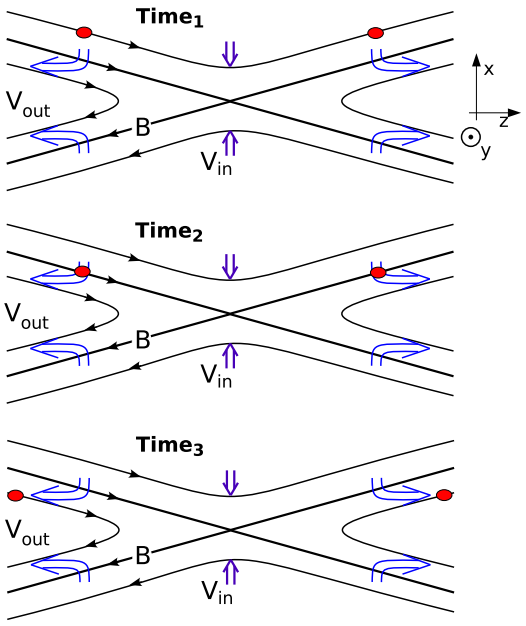

Figure 7.11: Sketch of the magnetic reconnection geometry and the associated plasma and magnetic flux transport.

General Properties and Definition

Magnetic reconnection implies a new connection of magnetic flux (or field lines) and therefore requires a violation of Ohm's law albeit in a very small region. Figure 7.11 illustrates the basic geometry and how magnetic flux and plasma is transported in a reconnection process. The thicker plotted magnetic field lines that cross in the center are called separatrices and the point where they cross is called an X-point or X-line (when the 3D aspect is emphasized). The blue arrows indicate qualitatively the plasma flow. The regions above and below the separatrices are called the inflow regions and the regions to the left and right are called the outflow regions. Although not required it can in general be assumed that the region at sufficient distance from the X line is ideal, i.e., that the frozen-in condition (Chapter 2) is satisfied.

The two red spots in the figure indicate plasma elements which are assumed to be at sufficient distance from the X-line such that the frozen-in condition applies to these elements. At time 1 both elements are connected by the same field line. At time 2 they are convected to the position of the X-line which implies that the magnetic field line on which they are located is now the new separatrix. At time 3 these elements are now in the outflow region and are located clearly on two separate magnetic field lines. Here the key property is the transport of the plasma elements from one side of the reconnection geometry (inflow region) across the separatrix into the outflow regions. This property can be used to identify or define magnetic reconnection:

Definition: Magnetic reconnection is a process in which plasma is transported across a separatrix surface.

It is important to note that this transport across a separatrix implies the violation of the frozen-in condition because plasma elements, which were originally connected by a field line, are later found on separate field lines. However, as mentioned this violation of the frozen-in condition is not required at the locations of

the plasma elements but only in a small vicinity of the X-line (in fact strictly it would be sufficient to have a violation of the frozen-in condition only at the X-line, although this is somewhat singular). To illustrate this point let us consider a representation of the two-dimensional magnetic field (in the x, z plane) by the y component of the vector potential $\mathbf{B} = \nabla A_y \times \mathbf{e}_y$ which implies $B_z = \partial A_y/\partial x$ and $B_x = -\partial A_y/\partial z$. For $B_z > 0$ for $z > 0$ (assumed in Figure 7.11) this implies that A_y has a local minimum at the X-line in a cut along x and a local maximum in a cut along z. In other words the X-point represents a saddle point for the vector potential A_y. Assuming a simple form of Ohm's law

$$\mathbf{E} = -\mathbf{u} \times \mathbf{B} + \eta \mathbf{j}$$

where the resistivity is nonzero only in the vicinity of the X-line. Using the vector potential the $y$component of Ohm's law can be written as

$$\frac{dA_y}{dt} = \frac{\partial A_y}{\partial t} + \mathbf{u} \cdot \nabla A_y = -\eta j_y$$

Noting that the current density at the X-line is negative $r = -\eta j_y|_{xl} > 0$ such that the change of the vector potential at the X-line is

$$\left.\frac{dA_y}{dt}\right|_{xl} = E_{y,xl} = r$$

Since this defines the separatrix, the value of A_y of the separatrix is increasing in time at a rate of r. Since $A_y$increases with x this implies field lines that have been originally in the inflow region will eventually become separatrices. Note also for fluid elements in the ideal plasma region Ohm's law implies

$$\frac{dA_y}{dt} = \frac{\partial A_y}{\partial t} + \mathbf{u} \cdot \nabla A_y = 0$$

in other words the value of the vector potential for the fluid element does not change along its path, i.e., $A_{y,fl} = \text{const}$. Thus if a fluid element is located at time 1 in the inflow region on a field line with $A_{y,fl} > A_{y,xl}$ at some later time 2 the A_y value of the X-line/separatrix will have increased to the value of $A_{y,fl}$ such that the plasma element is now located on the separatrix. As time continues $A_{y,xl}$ increases further such that the fluid element will be found in the outflow region.

Let us finally remark that this use of the vector potential is a straightforward measure of the magnetic flux in the two-dimensional plane, i.e., the amount of magnetic flux between two points $\mathbf{r}_a$ and $\mathbf{r}_b$ (assuming a unit length along the invariant direction y) is just the difference $\Phi_{ab} = A_y(\mathbf{r}_b) - A_y(\mathbf{r}_a)$. Hence the change of $A_{y,xl}$ is a direct measure of the amount of magnetic flux that is moved from the inflow region into the outflow region. The rate of the flux magnetic transport $r = -\eta j_y|_{xl}$ is called the reconnection rate.

Alternative definition: The 2D example illustrates that reconnection can also be identified/defined by the violation of the frozen-in condition at a X-line.

Finally it ought to be mentioned that there is considerable work on three-dimensional reconnection and associated concepts. A simple extension of the prior example which provides a little insight into 3D aspects is the assumption of a magnetic field into the plane (y direction). Note that the system still remains two-dimensional unless there is an actual variation along the y direction. A magnetic field would along y has almost no influence on the dynamics (it can be treated as an additional pressure term). The resulting geometry is more generic then the highly idealized case of strictly anti-parallel fields in our example which is singular in terms of actual applications. Since the dynamics in the x, z plane does not change everything in our discussion of reconnection remains valid applicable including the interpretation of the reconnection rate. However, with a B_y component the electric field at the X line is now along B_y whereas before this was a magnetic neutral line. From Ohm's law we know that the component of the electric field along the magnetic field must be 0 in an ideal plasma and thus there is a parallel electric field only in the vicinity of the X-line.

2nd alternative definition: We can use this property to postulate that three-dimensional magnetic reconnection is equivalent to the presence of an electric field parallel to the magnetic field in a sufficiently small region of space.

Note that this is a nontrivial property because $E_{\|} = \mathbf{E} \cdot \mathbf{B}/B$ is usually 0 in space plasma. This provides also a physically sound definition in the sense that $\mathbf{E} \cdot \mathbf{B}$ is a Lorentz invariant, i.e., the identification or definition of reconnection using this property is independent of the frame of reference. There are many more interesting aspects of reconnection in three dimensions which can found in the literature ... but for the purpose of this text it seems more important to discuss the actual dynamics of the more classical models of magnetic reconnection.

7.3.1 Reconnection models

In terms of analytic theory there are two main analytic approaches to the process of magnetic reconnection. One uses a steady state assumption for the local reconnection geometry and the other one treats reconnection as an instability (tearing mode) and addresses questions like the onset of reconnection. This instability aspect is more relevant for magnetotail dynamics.

Lundquist (or magnetic Reynolds number):

Ohm's law is of central importance for magnetic reconnection. In Chapter 2 we introduced general Ohm's law as

$$\mathbf{E} + \mathbf{u} \times \mathbf{B} = \frac{m_e m_i}{e^2 \rho} \left[\frac{\partial \mathbf{j}}{\partial t} + \nabla \cdot (\mathbf{u}\mathbf{j} + \mathbf{j}\mathbf{u}) \right] - \frac{M}{e\rho} \nabla \underline{\underline{\mathbf{p}}}_e + \frac{m_i}{e\rho} \mathbf{j} \times \mathbf{B} + \eta \mathbf{j} \tag{7.5}$$

with the resistivity $\eta = m_e \nu_c / n e^2$ where ν_c is the collision frequency between electrons and ions (or neutrals). Starting from general Ohm's Law this discussion focuses on the terms that can support an Electric field in the absence of plasma flow.

Lundquist number

Resistive Ohm's law:

$$\mathbf{E} = -\mathbf{u} \times \mathbf{B} + \eta \mathbf{j}$$

Using Ampere's law and the induction equation

$$\frac{\partial \mathbf{B}}{\partial t} = -\nabla \times \mathbf{E} = \nabla \times (\mathbf{u} \times \mathbf{B} - \eta \mathbf{j})$$

and for constant resistivity and assuming $\mathbf{u} = 0$:

$$\frac{\partial \mathbf{B}}{\partial t} = -\frac{\eta}{\mu_0} \nabla \times \nabla \times \mathbf{B} = \frac{\eta}{\mu_0} \Delta \mathbf{B} \tag{7.6}$$

Diffusion equation for magnetic field. The solution for specific initial/boundary conditions can be found easily through separation of variables. For the special case of a force free magnetic field

$$\mu_0 \mathbf{j} = \nabla \times \mathbf{B} = \alpha \mathbf{B}$$

with $\alpha = \text{const} = 1/L$ equation 7.6 reduces to

$$\frac{\partial \mathbf{B}}{\partial t} = \frac{\eta}{\mu_0} \Delta \mathbf{B} = -\frac{\eta}{\mu_0} \alpha^2 \mathbf{B}$$

with the solution

$$\begin{aligned} \mathbf{B}(\mathbf{r}, t) &= \mathbf{B}(\mathbf{r}, 0) \exp\left(-\frac{\eta t}{\mu_0 L^2}\right) = \mathbf{B}(\mathbf{r}, 0) \exp\left(-\frac{t}{\tau_{diff}}\right) \\ \text{with} \qquad & \tau_{diff} = \frac{\mu_0 L^2}{\eta} \end{aligned}$$

Normalization of 7.6 to identify typical diffusion time scale τ_{diff} using a typical system gradient length scale L yields the same result for τ_{diff}. Note that this is independent of the normalization of the magnetic field. Also since diffusion requires the presence of a current L can be interpreted as a typical current width (or half-width). This also allows to identify a velocity which corresponds to diffusion as $v_{diff} = L/\tau_{diff} = \eta/(\mu_0 L)$.

Another way to look at the problem of diffusion is to examine the distance a line of force can slip through the plasma in a given time τ. Using the above result this distance is

$$l_{diff} = \sqrt{\frac{\eta \tau}{\mu_0}}$$

We would like to set these diffusion properties (time and velocity) in relation to other typical time scales and velocities. In Chapter 2 we used a normalization that is based on the Alfven speed $v_A = B_0/\sqrt{\mu_0 \rho_0}$ and $\tau_A = L/v_A$. In fact when we use the Alfven speed and time for the normalization we obtain for the normalized Ohm's law

$$\widetilde{\mathbf{E}} = -\widetilde{\mathbf{u}} \times \widetilde{\mathbf{B}} + \widetilde{\eta}\widetilde{\mathbf{j}}$$

where $j_0 = B_0/\left(\mu_0 L\right)$ and $\widetilde{\eta} = \eta\tau_A/\left(\mu_0 L^2\right) = \tau_A/\tau_{diff}$. Another way to express this is in terms of the so-called Lundquist number

$$R = \frac{\tau_{diff}}{\tau_A} = \frac{1}{\widetilde{\eta}} = \frac{\mu_0 L^2}{\eta\tau_A} = \frac{\mu_0 L v_A}{\eta}$$

In a typical space plasma $R \gg 1$, i.e., diffusion is an incredibly slow process. Using the resistivity$\eta = m_e\nu_c/ne^2$and the definition of the electron skin depth the normalized resistivity becomes $\widetilde{\eta} = 1/R = \lambda_e^2\nu_c\tau_A/L_0^2$ and $\tau_{diff} = L_0^2/(\lambda_e^2\nu_c)$. Using typical values for the magnetopause, the near Earth magnetotail, and for the solar corona (for comparison) we obtain the following table which summarizes the basic plasma parameters and gives values for the collision frequency, the electron skin depth, the diffusion time, and the Lundquist number.

	Magnetopause	Magnetotail	Solar corona (flares)
n_0 [cm^{-3}]	4	0.5	$6 \cdot 10^8$
B_0 [nT]	40	20	$3 \cdot 10^7$
L_0 [m]	10^6	10^7	10^7
v_A [m/s]	$4.4 \cdot 10^5$	$6.2 \cdot 10^5$	$2.7 \cdot 10^7$
τ_A [s]	2.3	1.6	0.37
T_i [K]	10^6	$5 \cdot 10^7$	10^6
T_e [K]	10^5	$5 \cdot 10^6$	10^6
ω_{pe} [s^{-1}]	$1.1 \cdot 10^5$	$4.0 \cdot 10^4$	$1.4 \cdot 10^9$
Λ	$1.3 \cdot 10^{11}$	$1.3 \cdot 10^{13}$	$7 \cdot 10^7$
ν_c [s^{-1}]	$2 \cdot 10^{-7}$	10^{-9}	10
λ_e [m]	$2.7 \cdot 10^3$	$8.0 \cdot 10^3$	0.2
τ_{diff} [s]	$7 \cdot 10^{11}$	$1.5 \cdot 10^{15}$	$2.5 \cdot 10^{14}$
R	$3 \cdot 10^{11}$	10^{15}	10^{15}

The values demonstrate that in all three systems the Lundquist number is very large with a correspondingly large value for the diffusion time. Note that this is strictly not correct for the magnetopause and the magnetotail because the collision time $\tau_c = 1/\nu_{ei} \approx 10^7 - 10^9$s is much longer than the time a particle would spend at the magnetopause or in the magnetosheath.

7.3.2 Sweet-Parker Reconnection

This model has first been suggested by *Sweet* [1958] and independently by *Parker* [1957] and is based on a discussion of the pressure balance in the region of reconnection. In addition the model uses a classical resistivity (which can be substituted by other types of resistive interaction). The basic geometry is illustrated in Figure 7.12.

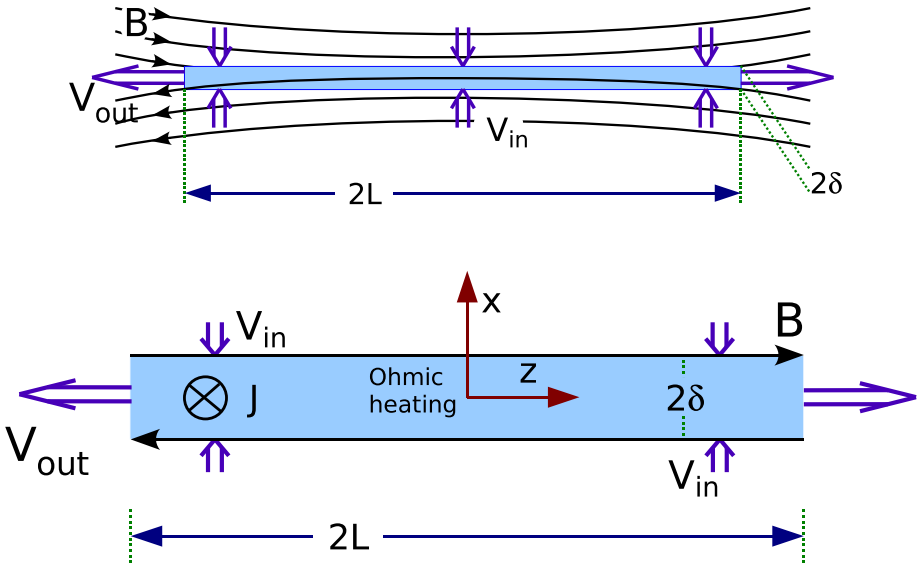

Figure 7.12: Illustration of the Sweet-Parker reconnection geometry. The top plot shows the overall geometry and the bottom plot illustrates the diffusion region.

The basic boundary conditions of this geometry are relatively straightforward. We assume that the diffusion region has a total length of L and total thickness of 2δ. At the inflow region we consider a magnetic field B_0 that is strongly tangential to the inflow boundary. The inflow velocity is approximately constant with a value of v_{in}. At the outflow boundary the magnetic field is B_{out} and the the outflow velocity is v_{out}. Note the the region inside the diffusion region is assumed to be dominated by diffusion where the outside region is assumed to be ideal. Other properties can be inferred from basic plasma physics. Total pressure balance $B^2/(2\mu_0) + p = \text{const}$ between the center of the diffusion region ($x = 0$) where the magnetic field is 0 and the inflow boundary implies

$$p_c - p_{in} = \frac{B_0^2}{2\mu_0}$$

Since the plasma is accelerated outward through $\mathbf{j} \times \mathbf{B}$ force the plasma velocity at the outflow boundary is

$$v_{out} = v_A = \frac{B_0}{\sqrt{\mu_0 \rho_{out}}}$$

Let us now consider the pressure equation for an MHD fluid (chapter 2)

$$\frac{1}{\gamma - 1}\left(\frac{\partial p}{\partial t} + \nabla \cdot p\mathbf{u}\right) = -p\nabla \cdot \mathbf{u} + \eta \mathbf{j}^2$$

$$\frac{dp}{dt} = \frac{\partial p}{\partial t} + \mathbf{u} \cdot \nabla p = -\gamma p \nabla \cdot \mathbf{u} + (\gamma - 1)\,\eta \mathbf{j}^2$$

Considering that (a) the dominant transport is along the current sheet (in the z direction), (b) the velocity increases linearly from 0 at the center to v_A at the outflow boundary, and (c) the current density is given by $j_0 = B_0/(\mu_0\delta)$ we can write the pressure equation for the central point of the diffusion region (where $u = 0$) as

$$\begin{aligned}\frac{\partial p_c}{\partial t} &= -\gamma p_c \nabla\cdot\mathbf{u} + (\gamma-1)\,\eta\mathbf{j}^2 \\ &= -\gamma p_c \frac{\Delta u_z}{L} + (\gamma-1)\,\eta\frac{B_0^2}{\mu_0^2\delta^2} \\ &= -\gamma\left(\frac{B_0^2}{2\mu_0}+p_{in}\right)\frac{v_A}{L} + (\gamma-1)\,\eta\frac{B_0^2}{\mu_0^2\delta^2}\end{aligned}$$

Assuming a steady pressure in the center of the diffusion region and $p_{in} = \lambda B^2/(2\mu_0)$ leads to

$$\frac{v_A}{L} = \frac{2(\gamma-1)}{\gamma(1+\lambda)}\frac{\eta}{\mu_0\delta^2}$$

or

$$\delta = \sqrt{\frac{2(\gamma-1)}{\gamma(1+\lambda)}\frac{\eta L}{\mu_0 v_A}} = \sqrt{\frac{2(\gamma-1)}{\gamma(1+\lambda)}}\frac{L}{\sqrt{R}}$$

with the Lundquist number $R = \mu_0 L v_A/\eta$ based on the length scale L. A relation for the inflow and outflow velocities can be obtained from the continuity equation (using constant density) by noting that the flux into the diffusion region must balance the flux out of the diffusion region

$$v_{in}L = v_A\delta \quad \text{or} \quad v_{in} = v_A\frac{\delta}{L} \approx v_A/\sqrt{R}$$

The resulting reconnection rate for the Sweet parker model is

$$E_{xl} = \eta j_{xl} = \eta\frac{B_0}{\mu_0\delta} = \frac{B_0 L v_A}{R\delta} \approx \frac{B_0 v_A}{\sqrt{R}}$$

Thus the reconnection rate normalized to the typical electric field $E_0 = B_0 v_A$ is

$$r = \frac{v_{in}}{v_A} \approx \frac{1}{\sqrt{R}}$$

Magnetic flux conservation can also be used to determine the magnetic field at the outflow boundary according to

$$v_{in}B_0 = v_A B_{out} \quad \text{or} \quad B_{out} = B_0 \frac{V_{in}}{v_A} = B_0/\sqrt{R}$$

Since the Lundquist or magnetic Reynolds number is typically a very large number, the resulting reconnection rate is very small. This implies also a very large aspect ratio L/δ. Note, however, that this still depends on the length scale L which is not necessarily fixed in this approach. While there may be geometrical arguments for a certain scale L the system could in principle realize a much smaller length L. For smaller L the Lundquist number becomes smaller $\sim L$ with a resulting larger reconnection rate.

Is the time $\tau_A = L/v_A$sufficient for magnetic field to diffuse of the distance δ? Using the diffusion length the diffusion length is

$$l_{diff} = \sqrt{\frac{\eta\tau_A}{\mu_0}} = \sqrt{\frac{\eta L}{\mu_0 v_A}} = \frac{L}{\sqrt{R}} = \delta,$$

i.e., consistent with the width of the diffusion region. It should be noted that this is not a self-consistent treatment of the reconnection problem or the diffusion region. The derived relations use a number of assumption and estimates most of which are straightforward such as pressure balance etc. However, other assumptions are not straightforward such as the constancy of the density, the precise flow profile, or the assumed length of the diffusion region L. The basic physics assumed in this model is relatively simple. The aspect ratio of the diffusion region is mostly fixed by the assumption of Ohmic heating ηj^2 and the required flow to maintain a constant pressure at the center of the diffusion region. If the diffusion region were wider compared to L the heating would be too small to sustain the flow. If it were narrower the heating would be too rapid resulting in an excess pressure violating the pressure balance requirement.

Alternative derivation: Consider Electric field in the inflow region $E_{in} = v_{in}B_0$ and electric field at the X-line $E_{xl} = \eta j_{xl} = \frac{\eta B_0}{\mu_0 \delta}$. With $E_{in} = E_{xl}$ we obtain

$$v_{in} = \frac{L}{\tau_{diff}} = \frac{\eta}{\mu_0 L}$$

which is the same as the diffusion velocity v_{diff} derived before. Using flux conservation $Lv_{in} = \delta v_{out}$ we can eliminate δ from the above equation

$$v_{in}^2 = \frac{\eta v_{out}}{\mu_0 L}$$

With $R = \mu_0 L v_A/\eta$ we obtain

$$v_{in}^2 = \frac{v_{out}v_A}{R}$$

or

$$r = M_{in} = \frac{v_{in}}{v_A} = \frac{\sqrt{v_{out}/v_A}}{\sqrt{R}}$$

where r is the dimensionless reconnection rate which is equal to the inflow Alfven Mach number M_{in}. From density and magnetic flux conservation we obtain:

$$\begin{aligned} \delta &= L\frac{v_{in}}{v_{out}} \\ B_{out} &= B_0\frac{v_{in}}{v_{out}} \end{aligned}$$

Now we have almost the same relations as in the prior derivation except for a specification of the outflow speed. To obtain the outflow speed let us consider the force balance along the z direction in steady state by assuming acceleration from $\mathbf{j}\times\mathbf{B}$ forces, i.e., $\rho\mathbf{u}\cdot\nabla\mathbf{u} = \mathbf{j}\times\mathbf{B}$ or

$$\rho\frac{v_{out}^2}{L} \approx \frac{B_0 B_{out}}{\mu_0\delta}$$

From flux conservation or $\nabla\cdot\mathbf{B} = 0$ we get $B_{out}/\delta = B_0/L$ such that

$$v_{out} = \frac{B_0}{\sqrt{\mu_0\rho}} = v_A$$

This yields the previous result for the reconnection flow and the aspect ratio:

$$v_{in} = \frac{v_A}{\sqrt{R}} \quad \text{and} \quad \frac{\delta}{L} = \frac{1}{\sqrt{R}}$$

This derivation did not make use of the pressure equation at all. Therefore it appears that the result is fairly robust and reflects more a scaling law rather than a concise treatment of the diffusion region. In fact, there is at present no self-consistent analytic solution for the diffusion region even though there have been many attempts. One complication is is illustrated considering the continuity and the pressure equations

$$\begin{aligned} \frac{\partial\rho}{\partial t} &= -\mathbf{u}\cdot\nabla\rho - \rho\nabla\cdot\mathbf{u} \\ \frac{\partial p}{\partial t} &= -\mathbf{u}\cdot\nabla p - \gamma p\nabla\cdot\mathbf{u} + (\gamma-1)\,\eta\mathbf{j}^2 \end{aligned}$$

Assuming a steady state solution at the stagnation point (X=line) where $\mathbf{u} = 0$ yields

$$\begin{aligned} 0 &= -\rho\nabla\cdot\mathbf{u} \\ 0 &= -\gamma p\nabla\cdot\mathbf{u} + (\gamma-1)\,\eta\mathbf{j}^2 \end{aligned}$$

Thus the continuity equation implies either $\rho = 0$ which is unphysical or $\nabla \cdot \mathbf{u} = 0$ at the X-line. However, the latter choice leads to $(\gamma - 1)\,\eta \mathbf{j}^2 = 0$. This implies either $\eta j^2 = 0$ which is not acceptable because it would imply that there is no electric field thereby contradicting the notion of reconnection; or it implies $\gamma = 1$ which means an isothermal system. This could be realized for instance by large thermal conductivity. Actually assuming a steady pressure makes sense because the pressure is forced to balance the magnetic pressure outside the diffusion region. This implies $\nabla \cdot \mathbf{u} = (\gamma - 1)\,\eta \mathbf{j}^2 / (\gamma p)$ at the X-line. using the result for the continuity equation at the X-line yields

$$\frac{1}{\rho_{xl}} \frac{\partial \rho_{xl}}{\partial t} = - \left. \frac{(\gamma - 1)\,\eta \mathbf{j}^2}{\gamma p} \right|_{xl}$$

with the solution

$$\begin{aligned} \rho_{xl}(t) &= \rho_{0,xl} \exp(-t/\tau_\rho) \\ with \qquad & \tau_\rho = \left. \frac{\gamma p}{(\gamma - 1)\,\eta \mathbf{j}^2} \right|_{xl} = \frac{\gamma}{2(\gamma - 1)} \tau_A \end{aligned}$$

where the $\tau_\rho has$been derived using the prior relations and the definition of the Lundquist number. Various attempts to model steady reconnection use incompressible dynamics which eliminates the pressure equation through the condition $\nabla \cdot \mathbf{u} = 0$. Formally this can be seen by the fact that the pressure contribution goes to 0 for $\gamma \to \infty$ in the total energy density (equation 6.17). This example demonstrates that a stationary solution may not be possible in the framework of the compressible MHD without either singularity at the X-line or without considering a heat flux or special values for γ.

7.3.3 Petschek Reconnection

As noted in the preceding section the long aspect ratio limits the possible reconnection rate in the Sweet-Parker model. *Petschek* [1964] realized that a much larger reconnection rate would be possible if the diffusion region were much shorter. In fact, as noted earlier the diffusion electric field needs to be present only in a very small vicinity of the X-line. A long and narrow diffusion region implies that all flow must go through the narrow channels as illustrated for the flux of mass and magnetic field.

Figure 7.13 illustrates the basic reconnection geometry that Petschek suggested. The main point in Petschek's model is that the length of the diffusion region should be much shorter $L_p \ll L$ in order to realize a higher reconnection rate. The basic scaling in his model is illustrated in Figure 7.13. Note that a much shorter diffusion region also implies a thinner diffusion region, i.e., $\delta_p \ll \delta$. The fast transport out of this diffusion region over the scale from L_p to L occurs through a flow layer which is bounded by slow shocks.

Let us first look at the scaling in the vicinity of the diffusion region. The magnetic field in the inflow of the Petschek region is denoted B_p which is smaller than B_0. However, since we have magnetic flux conservation $v_{in} B_0 = v_{in,p} B_p$ (and assuming constant mass density) the inflow Alfven Mach number relate with $v_{A,p} = B_p / \sqrt{\mu_0 \rho} = v_A B_p / B_0$ as

$$\frac{M_{in}}{M_{in,p}} = \frac{B_p^2}{B_0^2}$$

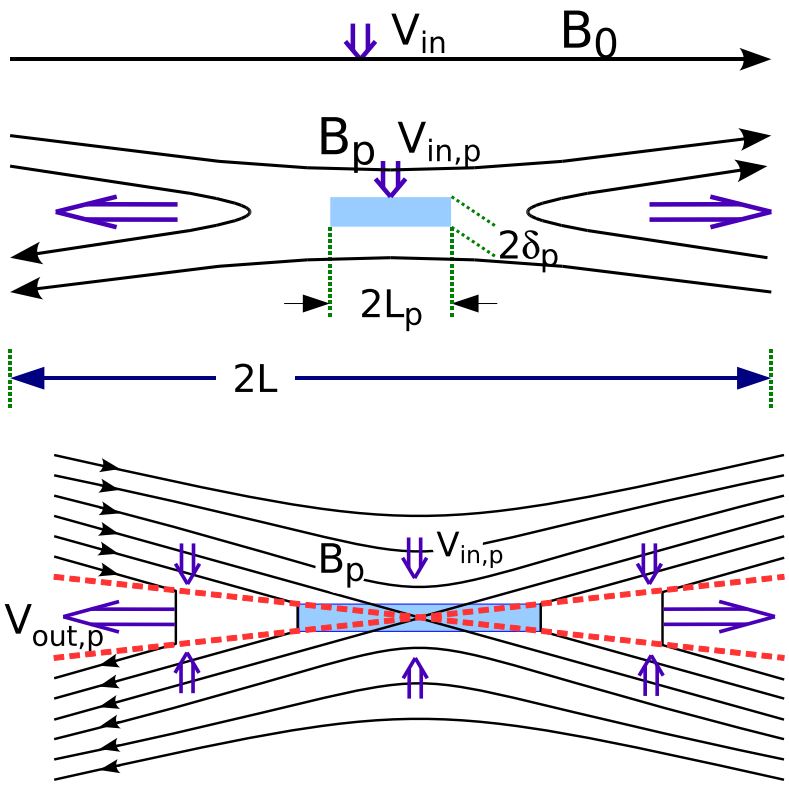

Figure 7.13: Illustration of the Petschek reconnection geometry. Top: Scales assumed in Petschek's model; Bottom: illustration of the diffusion region and the attached slow shocks.

For the length scale we obtain with $R = \mu_0 L v_A/\eta$ and $R_p = \mu_0 L_p v_{A,p}/\eta$

$$\frac{L_p}{L} = \frac{R_p}{R}\frac{v_A}{v_{A,p}} = \frac{1}{R}\frac{v_{A,p}^2}{v_{in,p}^2}\frac{B_0}{B_p} =$$

with $B_0/B_p = M_{in,p}^{1/2}/M_{in}^{1/2}$ we obtain

$$\frac{L_p}{L} = \frac{1}{R}\frac{1}{M_{in,p}^{3/2}}\frac{1}{M_{in}^{1/2}}$$

and

$$\frac{\delta_p}{L} = \frac{L_p}{L}\frac{1}{\sqrt{R_p}} = \frac{1}{R}\frac{1}{M_{in,p}^{3/2}}\frac{1}{M_{in}^{1/2}}M_{in,p} = \frac{1}{R}\frac{1}{M_{in}^{1/2}}\frac{1}{M_{in,p}^{1/2}}$$

Thus, once we have determined B_p/B_0we can obtain the ratio of the inflow Mach numbers as well as the scale of the Petschek diffusion region. Note that this is really just a re-scaling of the diffusion region in

size and is applicable to any smaller scale diffusion region. It should also be remarked that similar to the Sweet-Parker model, this model of reconnection does not treat the diffusion region self-consistently.

The main insight from Petschek was that the the transport from L_p to L does not require the thin outflow layer. Petschek suggested that the outflow region is bounded by two slow switch-off shocks (thick red lines in Figure 7.13). Note that this is strictly only true if the shocks are horizontal, i.e., aligned with the z direction. However, since the shocks are only very slightly inclined the error in the assumption of switch-off shocks is small. From the discussion of switch-off slow shocks we know that in the de-Hoffmann-Teller frame (in which the flow is field-aligned) the upstream velocity is $u_u = v_{Au}$ (equation 6.84) such that the tangential and normal components of the upstream velocity are

$$\begin{aligned} u_{tu} &= \frac{B_{tu}}{\sqrt{\mu_0 \rho_u}} = v_{At} \\ u_{nu} &= \frac{B_n}{\sqrt{\mu_0 \rho_u}} = v_{An} \end{aligned}$$

However, the rest frame of the diffusion region is not the de-Hoffmann-Teller (dHT) frame. In the rest frame the flow is almost normal to the shock. Therefore the transformation into the dHT frame requires to add a velocity of $u_t = v_{At}$ to the rest frame. In other words the plasma in the outflow region must be jetting at the speed of

$$v_{out,p} = v_{At,p} \approx B_p / \sqrt{\mu_0 \rho}$$

away from the diffusion region to satisfy the switch-off shock conditions. Secondly it should be noted that the actual normal velocity in the downstream (outflow) region is 0. This means that the slow shock is moving with a velocity u_{nu} toward the upstream (inflow) region.

The prior discussion assumes that the density is constant, which is incorrect for a slow shock. In fact we can compute the outflow density from the switch-off shock properties. To do so one has to determine the angle of the upstream magnetic field with the shock normal. The tangential component of this field is B_p and the normal component is B_n. Magnetic flux conservation implies $v_{nu} B_p = v_{At,p} B_n$ such that

$$\tan\theta = \frac{B_n}{B_p} = \frac{v_{nu}}{v_{At,p}} = r_p$$

where r_p is the reconnection rate for the Petschek diffusion region. This illustrates that $\theta \approx r_p \ll 1$ such that the compression is approximately $X = 1 + \left(2c_s^2/v_{A,p}^2 + \gamma - 1\right)^{-1}$. The resulting maximum compression occurs for $c_s^2 \ll v_{A,p}^2$ with $X = 5/2$. This result can be utilized to correct the Sweet-Parker discussion of the diffusion region for different in- and outflow densities. Using mass conservation the Sweet-Parker reconnection rate is corrected to

$$\frac{v_{in}}{v_A} = \left(\frac{\rho_{out}}{\rho_{in}}\right)^{1/4} \left(\frac{\eta}{\mu_0 L v_A}\right)^{1/2} = \left(\frac{\rho_{out}}{\rho_{in}}\right)^{1/4} \frac{1}{\sqrt{R}}$$

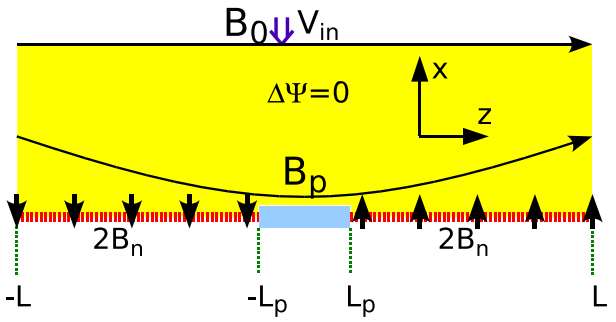

Figure 7.14: Sketch of the inflow field solution in Petschek's model.

(e.g. Priest, 2000) such that the actual change in the reconnection rate is rather small and we can ignore this correction for the Petschek mechanism.

Finally it is important to determined the magnetic field at the diffusion region B_p. This field is modified because the field in the vicinity of the diffusion region is curved and different from the field B_0 at large distance from the diffusion region (Figure 7.14). The field perturbation $\mathbf{B}_c$in the inflow region is assumed to by derived from a potential Ψ (such that $\nabla \times \mathbf{B}_c = 0$). At the slow shocks the magnetic field should be B_n, however, here the shocks have an inclination of $\delta_p/L_p = v_{in,p}/v_{A,t} = B_n/B_p$ with the z axis. To account for this we actually need a boundary value of $2B_n$ for the magnetic field correction in the inflow region from $-L$ to $-L_p$ and from L_p to L along the z axis. Projected onto the slow shock with the inclination B_n/B_p this yields a normal magnetic field of B_n. Assuming that the field is generated from a continuous series of monopoles along the shocks (red line in Figure 7.14, the field correction from the monopoles observed at $\mathbf{r}_0$ from a line element dz at $\mathbf{r} = (0, z)$ is then

$$d\mathbf{B}_c = \frac{2B_n\left(\mathbf{r}_0 - \mathbf{r}\right)}{\pi\left(\mathbf{r}_0 - \mathbf{r}\right)^2}dz$$

The total field correction is obtained by integrating along the z axis

$$\mathbf{B}_c = \frac{2B_n}{\pi}\left(-\int_{-L}^{-L_p}\frac{\left(\mathbf{r}_0 - \mathbf{r}\right)dz}{\left|\mathbf{r}_0 - \mathbf{r}\right|^2} + \int_{L_p}^{L}\frac{\left(\mathbf{r}_0 - \mathbf{r}\right)dz}{\left|\mathbf{r}_0 - \mathbf{r}\right|^2}\right)$$

where the minus sign in the first term is to generate $-2B_n$ for $z < 0$. To illustrates this let us take as an example a sheet of monopoles from $-d$ to $+d$ along the z axis. The x component (normal) of the field observed at $\mathbf{r}_0 = (x_0, y_0)$is

$$\begin{aligned}\mathbf{B}\left(x_0, z_0\right) &= \frac{2B_n}{\pi}\left(\int_{-d}^{d}\frac{x_0 dz}{\left|\mathbf{r}_0 - \mathbf{r}\right|^2}\right) = \frac{2B_n}{\pi}x_0\left(\int_{-d}^{d}\frac{dz}{x_0^2 + \left(z_0 - z\right)^2}\right) \\ &= \frac{2B_n}{\pi}x_0\left(\int_{-d-z_0}^{d-z_0}\frac{d\tilde{z}}{x_0^2 + \tilde{z}^2}\right) = \frac{2B_n}{\pi}x_0\frac{1}{x_0}\left(\arctan\frac{d - z_0}{x_0} - \arctan\frac{-d - z_0}{x_0}\right)\end{aligned}$$

Considering the limit $x_0 \to 0$ for $-d < z_0 < d$ yields $B_x(0, z_0) = 2B_n$ as expected. Using now the monopole distribution of Figure 7.14 and computing the z component in the center of the diffusion region yields the desired correction to the magnetic field in the inflow region:

$$\begin{aligned} B_{z,c} &= \frac{2B_n}{\pi}\left(\int_{-L}^{-L_p}\frac{dz}{z} - \int_{L_p}^{L}\frac{dz}{z}\right) \\ &= \frac{2B_n}{\pi}\left(\ln\frac{L_p}{L} - \ln\frac{L}{L_p}\right) = -\frac{4B_n}{\pi}\ln\frac{L}{L_p} \end{aligned}$$

Adding this field to the homogeneous field yields the magnetic field at the diffusion region

$$B_p = B_0 - \frac{4B_n}{\pi}\ln\frac{L}{L_p} = B_0\left(1 - \frac{4M_{in}}{\pi}\ln\frac{L}{L_p}\right)$$

For $\frac{4M_{in}}{\pi}\ln\frac{L}{L_p} \leq 1/2$ the above expression implies $B_p \approx B_0$ such that $M_{in,p} \approx M_{in}$ and the relations for the diffusion region scales become

$$\frac{L_p}{L} = \frac{1}{R}\frac{1}{M_{in}^2} \qquad \frac{\delta_p}{L} = \frac{1}{R}\frac{1}{M_{in}}$$

Petschek suggested that the process becomes inefficient if B_p becomes too small. Assuming that a reasonable value for the minimum B_p is $B_p \approx B_0/2$ yields for the approximate maximum inflow Mach number (or reconnection rate)

$$M_{in} = r_p \approx \frac{\pi}{8\ln(L/L_p)} = \frac{\pi}{8\ln(M_{in}^2 R)} \approx \frac{\pi}{8\ln R}$$

This reconnection rate is much larger than the Sweet-Parker rate. For instance for a Lundquist number of $R = 10^8$ the Petschek reconnection rate is $r_p \approx 2 \cdot 10^{-2}$ compared to a Sweet-Parker rate of $r_{sp} \approx 10^{-4}$. The reason is as stated that the aspect ratio δ_p/L_p is much larger than δ/L for the Sweet-Parker diffusion region. This is accomplished by a much smaller length of the diffusion region $L_p \approx L64\ln^2 R/(\pi^2 R)$. However, it is also important to note that the thickness of the Petschek diffusion region is much smaller $\delta_p \approx \delta 8\ln R/\left(\pi\sqrt{R}\right)$. This is required because the larger reconnection rate must be equivalent to a larger electric field $E_{xl} = \eta j_{xl} = \eta B_p/(\mu_0\delta_p)$ which requires a $\delta_p \ll \delta$. This concept of reconnection is remarkably simple and it was able to explain many observations in terms of magnetic reconnection where the Sweet-Parker rate was far too small.

Another important aspect is the near scale invariance of Petschek reconnection. If the inflow magnetic field $B_0$and density ρ_0 are given, the Sweet-Parker range obviously depends on the scale L. However, since the Petschek rate depends only on $\ln R$, it various only between 0.09 and 0.01 for Lundquist numbers ranging from 10^2 to 10^{20} such that a value of $r_p \approx 3 \cdot 10^{-2}$ is a reasonable representation for most plasmas. With Ohm's law this also implies that $\delta_p \approx \eta/(\mu_0 r_p v_A)$ which is fairly insensitive to the macroscopic length scale L.

7.3.4 Application and Further Discussion of Magnetic Reconnection

Diffusion and Reconnection Parameters or the Giant Sliced by a String

Magnetic reconnection is important in many different space plasma systems. A key issue for reconnection models are their properties applied to particular systems and how these compare to actual observations. The following table lists various typical parameters for diffusion, Sweet-Parker reconnection and Petschek reconnection applied to the magnetopause, the magnetotail, and flares in the solar corona.

	Magnetopause	Magnetotail	Solar corona (flares)
n_0 [cm^{-3}]	4	0.5	$6 \cdot 10^8$
B_0 [nT]	40	20	$3 \cdot 10^7$
L [m]	10^6	10^7	10^7
v_A [m/s]	$4.4 \cdot 10^5$	$6.2 \cdot 10^5$	$2.7 \cdot 10^7$
$E_0 = v_A B_0$ [V]	$1.8 \cdot 10^{-2}$	$1.3 \cdot 10^{-2}$	$8 \cdot 10^5$
τ_A $[s]$	2.3	1.6	0.37
v_{thi} $[K]$	10^5	$7 \cdot 10^5$	10^5
v_{the} $[K]$	$1.3 \cdot 10^6$	10^7	$4.3 \cdot 10^6$
λ_e [m]	$2.7 \cdot 10^3$	$8.0 \cdot 10^3$	0.2
τ_{diff} $[s]$	$7 \cdot 10^{11}$	$1.5 \cdot 10^{15}$	$2.5 \cdot 10^{14}$
R	$3 \cdot 10^{11}$	10^{15}	10^{15}
r_{sp}	$1.8 \cdot 10^{-6}$	$3 \cdot 10^{-8}$	$3 \cdot 10^{-8}$
r_p	$1.5 \cdot 10^{-2}$	$1.1 \cdot 10^{-2}$	$1.1 \cdot 10^{-2}$
r_{obs}	$3 \cdot 10^{-2}$	$3 \cdot 10^{-2}$	$10^{-4}$to 10^{-2}
δ_{sp} [m]	1.8	0.3	0.3
δ_p [m]	$2 \cdot 10^{-4}$	10^{-6}	10^{-6}
L_p [m]	$1.4 \cdot 10^{-2}$	10^{-4}	10^{-4}

The table demonstrates that particularly the values for the observed reconnection rates are much more realistic for the Petschek model. However, it also illustrates that the dimensions of the Petschek diffusion region are awfully small based on Coulomb collisions. We will return to this issue in a moment. In fact when considering the gigantic scales of magnetospheric or solar magnetic field of ten thousands of km and assuming that these field are reconnected on a potential fast time scale in a region that has some 10^{-6} to 10^{-2} m in size is difficult to imagine. However before we attend to this problem in more detail let us look at some other properties.

The next table shows typical time scales and velocities associated with diffusion, Sweet-Parker and Petschek reconnection. Here velocities refer to the inflow velocity and the time scales denote the time needed to reconnect magnetic flux in a layer of thickness L. Again the table illustrates that times for diffusion and Sweet-Parker reconnection are extremely long and the corresponding velocities are unrealistically small. Vice versa Petschek reconnection appears to produce realistic times and reconnection velocities for all three systems.

	Magnetopause	Magnetotail	Solar corona (flares)
L [m]	10^6	10^7	10^7
v_A [m/s]	$4.4 \cdot 10^5$	$6.2 \cdot 10^5$	$2.7 \cdot 10^7$
τ_A $[s]$	2.3	1.6	0.37
R	$3 \cdot 10^{11}$	10^{15}	10^{15}
τ_{diff} $[s]$	$7 \cdot 10^{11}$	$1.5 \cdot 10^{15}$	$2.5 \cdot 10^{14}$
τ_{sp} $[s]$	10^6	$5 \cdot 10^7$	10^7
τ_p $[s]$	150	150	35
v_{diff} [m/s]	$1.5 \cdot 10^{-6}$	$6 \cdot 10^{-10}$	$2.7 \cdot 10^{-8}$
v_{sp} [m/s]	0.8	0.02	0.1
v_p [m/s]	$3 \cdot 10^3$	$5.5 \cdot 10^3$	$2.5 \cdot 10^5$

Diffusion Region Physics - Anomalous Resistivity or a Bigger String

There have been many attempts to improve Petschek's reconnection [*Valyliunas*, 1975; *Priest and Forbes*, 2000], however, there is to-date no self-consistent treatment off the diffusion region. We pointed out one possible problem in the different dynamics of continuity and pressure equation. A much discussed topic is the length of the diffusion region. Petschek argued that the diffusion region adjusts in order to realize a large reconnection rate. However, for constant resistivity many numerical simulation and some analytic estimates indicate that in the opposite, an initially short diffusion rate may in fact lengthen and lead to a lower reconnection rate approach the Sweet-Parker rate as time continues. Another issue with the application of both, Sweet-Parker and Petschek reconnection is the width of the diffusion region. The above table illustrates that this is of the order of meters for the considered applications for Sweet-Parker reconnection and of the order of 10^{-4} to 10^{-6}m for Petschek reconnection. Clearly there seems to be something odd about this. To shed more light on this issue let us compute the drift speed that is necessary to maintain the current for Sweet-Parker reconnection.

$$\begin{aligned} j &= ne\left(v_{di} - v_{de}\right) = \frac{B_0}{\mu_0 \delta} \quad or \\ v_{di} - v_{de} &= \frac{B_0}{\mu_0 ne\delta} = \frac{B_0}{\sqrt{\mu_0 m_i n}} \frac{c\left(\epsilon_0 m_i\right)^{1/2}}{\left(\mu_0 ne^2\right)^{1/2} \delta} = v_A \frac{c}{\omega_{pi}\delta} \end{aligned}$$

In other words $v_{di} - v_{de} = v_A \lambda_i / \delta$. Here $\lambda_i = \lambda_e \sqrt{m_i/m_e}$ is the ion inertial length which is 100 km, 400 km, and 10 m for the magnetopause, the magnetotail, and the solar corona respectively. his illustrates that the relative drift speed approaches the Alfvén speed when the diffusion region width becomes the ion inertial length. Clearly the Sweet-Parker and the Petschek diffusion region widths based on Coulomb collisions are already much thinner then λ_i such that the current drift speed exceed the Alfvén speed by orders of magnitude. We gain still more insight by comparing the drift speed with the ion thermal velocity.

$$\frac{v_{di} - v_{de}}{v_{thi}} = \frac{v_A}{v_{thi}} \frac{\lambda_i}{\delta}$$

The current drift speed equals the ion thermal speed for

$$\delta = \delta_i = \frac{\lambda_i v_A}{v_{thi}}$$

The significance of this is that current sheets thinner then δ_i implies drift speeds in excess of the ion thermal speed can be expected to generate micro-instabilities. The turbulent interaction of the waves with the current carrying particles will slow the particle to conditions sub-critical for the instability. Typical instabilities discussed in this context are the lower hybrid drift instability, the ion acoustic instability, the modified two-stream (Buneman) instability, and ion or electron cyclotron waves. The precise onset conditions for these instabilities vary and depend on the magnetic field and plasma configuration. The actual onset of the instabilities requires often a somewhat higher drift speed, foe instance the ion acoustic instability either requires a significantly higher drift speed or a much higher electron temperature. A reasonable minimum requirement for the onset of strong turbulence through micro-instabilities could require the drift speed to exceed the electron thermal velocity

$$\frac{v_{di} - v_{de}}{v_{the}} = \frac{v_A}{v_{the}} \frac{\lambda_i}{\delta}$$

which yields the condition for onset

$$\delta = \delta_e = \frac{\lambda_i v_A}{v_{the}}$$

We can now use the results for Sweet-Parker and Petschek reconnection to infer the necessary Lundquist number and the collision frequency. With $R = \tau_{diff}/\tau_A = L^2/(\lambda_e^2 \nu_c \tau_A)$ Sweet parker reconnection yields

$$\frac{\delta}{L} = \frac{1}{\sqrt{R}} = \frac{\lambda_e}{L}\sqrt{\nu_{sp}\tau_A}$$

Using the current constraints δ_i and δ_e and solving for the required collision frequencies yields

$$\nu_{sp,i} = \frac{m_i v_A^2}{\tau_A m_e v_{thi}^2} \quad \text{and} \quad \nu_{sp,e} = \frac{m_i v_A^2}{\tau_A m_e v_{the}^2}$$

for the frequencies corresponding to δ_i and δ_e respectively. Using $\delta/L = R^{-1/2}$ and solving for the Lundquist numbers yields

$$R_{sp,i} = \frac{L^2}{\lambda_i^2}\frac{v_{thi}^2}{v_A^2} \quad \text{and} \quad R_{sp,e} = \frac{L^2}{\lambda_i^2}\frac{v_{the}^2}{v_A^2}$$

For Petschek reconnection $\delta_p/L = 1/(rR)$ and $R = \tau_{diff}/\tau_A = L^2/(\lambda_e^2 \nu_c \tau_A)$ with the constraints δ_i and $\delta_e$we have

$$\frac{1}{rR} = \frac{\lambda_i v_A}{L v_{thi}} \quad \text{or} \quad = \frac{\lambda_i v_A}{L v_{the}}$$

Solving for the required anomalous collision frequency

$$\nu_{p,i} = r\frac{\lambda_i v_A^2}{\lambda_e^2 v_{thi}} \quad \text{and} \quad \nu_{p,e} = r\frac{\lambda_i v_A^2}{\lambda_e^2 v_{the}}$$

corresponding to δ_i and δ_e respectively. Similarly the Lundquist numbers for the current constraints and Petschek reconnection are

$$R_{p,i} = \frac{1}{r}\frac{L v_{thi}}{\lambda_i v_A} \quad \text{and} \quad R_{p,e} = \frac{1}{r}\frac{L v_{the}}{\lambda_i v_A}$$

Results for these reconnection parameters assuming a current limitation are given in the following table.

	Magnetopause	Magnetotail	Solar corona (flares)
L [m]	10^6	10^7	10^7
v_A [m/s]	$4.4 \cdot 10^5$	$6.2 \cdot 10^5$	$2.7 \cdot 10^7$
τ_A $[s]$	2.3	1.6	0.37
v_{thi} $[K]$	10^5	$6.2 \cdot 10^5$	10^5
v_{the} $[K]$	$1.3 \cdot 10^6$	10^7	$4.3 \cdot 10^6$
λ_i [m]	$1.2 \cdot 10^5$	$3.4 \cdot 10^5$	8.6
λ_e [m]	$2.7 \cdot 10^3$	$8.0 \cdot 10^3$	0.2
δ_i [m]	$5.3 \cdot 10^5$	$3.4 \cdot 10^5$	$2.3 \cdot 10^3$
δ_e [m]	$4.1 \cdot 10^4$	$2.1 \cdot 10^4$	54
L/λ_i	8.3	29	$1.2 \cdot 10^6$
L^2/λ_i^2	69	870	$1.4 \cdot 10^{12}$
L^2/λ_e^2	$1.4 \cdot 10^5$	$1.6 \cdot 10^6$	$2.5 \cdot 10^{15}$
$R_{sp,i}$	3.6	870	$1.9 \cdot 10^7$
$R_{sp,e}$	600	$2.3 \cdot 10^5$	$3.6 \cdot 10^{10}$
$\nu_{sp,i}$ $[s^{-1}]$	$1.5 \cdot 10^4$	$1.1 \cdot 10^3$	$5.0 \cdot 10^7$
$\nu_{sp,e}$ $[s^{-1}]$	91	4.4	$2.0 \cdot 10^5$
τ_{diff} $[s]$	$7 \cdot 10^{11}$	$1.5 \cdot 10^{15}$	$2.5 \cdot 10^{14}$
$R_{p,i}$	14	410	$6.3 \cdot 10^6$
$R_{p,e}$	360	$9.4 \cdot 10^3$	$4.1 \cdot 10^8$
$\nu_{p,i}$ $[s^{-1}]$	320	$3.4 \cdot 10^3$	$3.6 \cdot 10^9$
$\nu_{p,e}$ $[s^{-1}]$	24	210	$8.3 \cdot 10^7$
$L^2/\left(\lambda_e^2 \tau_A\right)$	$6.1 \cdot 10^4$	10^6	$6.8 \cdot 10^{15}$
$r_{sp,i}$	0.8	$6 \cdot 10^{-2}$	$7 \cdot 10^{-4}$
$r_{sp,e}$	$6 \cdot 10^{-2}$	$1.5 \cdot 10^{-2}$	$1.1 \cdot 10^{-4}$
$r_{p,i}$	0.13	$7 \cdot 10^{-2}$	$3 \cdot 10^{-2}$
$r_{p,e}$	$7 \cdot 10^{-2}$	$5 \cdot 10^{-2}$	$2 \cdot 10^{-2}$

The derived parameters shed much light on the physics needed to maintain either the Sweet-Parker of the Petschek reconnection geometry. The basic idea behind these parameters is rather simple in that it is assumed that the current width of the diffusion region cannot collapse below a meaningful physical length scale. The criterion applied uses a current limitation based on the generation of strong turbulence which is assumed to inhibit any further reduction in the width of the current in the diffusion region.

Since the limiting width scales with λ_i, it is not surprising that the Lundquist numbers for the different cases involve the factor L/λ_i. I should also be noted that the required collision frequencies for Sweet-Parker reconnection are not scale independent but are proportional to $1/\tau_A = v_A/L$. In contrast the collision frequencies for Petschek reconnection are indeed mostly independent of L (there is a weak logarithmic dependence through the actual reconnection rate r). In other words, if reconnection occurs on a fast time scale and the diffusion region width is limited by the current that can flow through the region, the required anomalous collision frequencies are fixed within a certain range (depending on the details of the current limitation).

Considering the values in the above table a number of properties are noteworthy: The current limitation anomalous collision frequencies many orders of magnitude higher then the actual coulomb collision

frequencies. For the magnetopause and the magnetotail the resulting reconnection rates of Sweet-Parker reconnection and Petschek reconnection are fairly comparable. The reason for this is that for these current systems the macroscopic scale is only one or two orders of magnitude larger then the current limitation scale δ_i or δ_e. It should be remarked that for the magnetosphere the scale $\delta_e$is probably the more relevant scale because the onset condition for micro-instabilities is usually closer to the electron thermal speed. It should also be remarked that reconnection rates close to 1 are unrealistic. They would imply that the aspect ratio is close to one which implies a separatrix angle of 45°. However, for such an angle the magnetic field at the X-line can be constructed from a vacuum field, i.e., there is no or very little current at the X-line at which point reconnection must switch of. In summary, the current limitation leads to more realistic scale of the diffusion region but it is still impressive that regions of the size of a few 10 meters (for the corona) or a few 10 km (magnetosphere) can generate all the reconnection that is need in very large scale system to reconnect a major amount of the magnetic flux in the system.

Diffusion Region Physics - Length of the Diffusion Region

In terms of the observations it is not clear that reconnection occurs everywhere on a fast Petschek-like rate. However, there is clear evidence that reconnection particularly in the magnetosphere does often occur with a fast reconnection rate.

This previous section poses some fundamental new questions. Most strikingly the current limitation does not provide a unique answer to the actual collision frequency. This is clearly demonstrated for the solar applications. Here the current limitation applied to Sweet-Parker and Petschek reconnection uses the same width but yields different anomalous collision frequencies, Lundquist numbers, and reconnection rates. The basic difference here is the length of the assumed diffusion region. The long Sweet-Parker diffusion region leads to a much slower diffusion-like process for the same current width as the shorter Petschek diffusion region. This poses the question as to what determines the length of the diffusion region? There has been much research on this point which examines these processes often in relation to particular in- and outflow boundary conditions.

While this work sheds some important new light on reconnection it is not clear, how particular boundary conditions can be applied to a reconnection process at the magnetopause or the sun where diffusion regions of reconnection occupy only a minute fraction of the overall volume.

There are several aspects of recent research that are important important for the physics of the diffusion region. So far the discussion had assumed that the resistivity is constant and numerical simulation in deed support the result that the diffusion region tends to lengthen in simulations even if it is initially set up to be short to support Petschek-type reconnection. However, if the resistivity is caused by turbulence the assumption of constant resistivity is not anymore correct. Since the turbulence is driven by the strength of the current density the resistivity becomes current dependent. This in fact has shown the result in simulations that the diffusion region stays much shorter and reconnection is fast as suggested by Petschek.

In recent year there has been a new development in that the inclusion of the Hall term appears to have a strong influence on reconnection. In fact it was found in a simple numerical reconnection experiment that different plasma approximation (Hall MHD, Two-fluid plasma, Hybrid simulations with ions as particles and electrons as fluid, and full particle simulations) all show approximately the same fast reconnection rate[*Birn et al.*, 2001; *Otto*, 2001; *Shay et al.*, 2001]. While details in the reconnection geometry were

different in these simulations they all showed a short diffusion region (few ion inertia lengths) and a width that was some fraction of ion inertial length. This finding was in contrast to pure MHD models where the diffusion region tended to lengthen with a lower reconnection rate. The common physics in all models with fast Petschek-like reconnection was the inclusion of Hall Physics.

The physics of the diffusion region including the Hall term in Ohm's law is more complicated. One of the most important aspects is that the frozen-in condition now applies to the electrons in the plasma. The electrons also carry much of the current in the diffusion region and are moving into the y direction (into the plane in 2D reconnection) So, during their acceleration out of the diffusion region they not only move along z but also in y. Since the magnetic field is moving with the electrons magnetic field lines in the symmetry plane ($x = 0$) now are displaced (bent) along y which means that different from MHD now there are in- and out-of plane magnetic field and flow components. This rotation of the magnetic field is known for whistler wave and whistler wave are in fact facilitated through the inclusion of the Hall term. So the build up of a very characteristic pattern of B_y magnetic field is typical for Hall reconnection. However, this in turn provides another argument for the limitation of the length of the diffusion region. If the diffusion region were long and thin the current density would be high of a large distance along the diffusion region. This would generate very strong B_y flux over an extended region along the diffusion region. However, this generation requires energy and allows that the process can operate only of a limited length thereby providing a limitation of the length of the diffusion region.

Finally it should be noted that there are still other aspects that can play a role. Simulations indicate that the other terms in general Ohm's law can contribute to the reconnection electric field. Specifically the electron pressure tensor and the electron inertial term. Currently there is no final conclusion regarding these problems of the physics of the diffusion region. This is in part also because the real world is three-dimensional which contributes additional complication and becomes a computational challenge particularly for particle simulations. It not unlikely that there is no unique answer to the reconnection problem and that it really depends on the specific plasma parameters and the geometry of the current layers. For instance it is well known and easy to demonstrate the plasma flow in the inflow regions can alter the reconnection rate and structure of the reconnection geometry. For instance if flow along the magnetic field in the inflow regions surpasses the Alfvén speed reconnection must shut off. The information that reconnection operates is transmitted at Alfvén speed and if the plasma in the inflow region is jetting faster this information cannot spread such the reconnection is switched-off.

Fortunately for many applications of reconnection, the details of the diffusion region may not matter too much as long as a model approximates the reconnection rate sufficiently well. Since the diffusion region occupies only a tiny volume of the overall configuration, all large scale feature such as mass, momentum, energy, and magnetic flux transport are reasonably approximated if a uses a good approximate too the reconnection rate independent of details in the diffusion region.

7.3.5 Observation of magnetopause reconnection

The observational verification of reconnection is difficult because a satellite provides only point measurements of usually complex plasma structure. Two major signatures are used to identify reconnection at the magnetopause.

(a) On macro scales reconnection should generate open magnetic field which implies that the magnetopause is at time approximately a rotational discontinuity. In this case measurements of the plasma

velocity and magnetic field should satisfy approximately the so-called Walen relation

$$\Delta\mathbf{u} = \pm\Delta\mathbf{v}_A = \pm\Delta\frac{\mathbf{B}}{\sqrt{\mu_0\rho}}.$$

Where $\Delta\mathbf{u} = \mathbf{u} - \mathbf{u}_{ref}$ with a measure velocity $\mathbf{u}$ and a reference measurement $\mathbf{u}_{ref}$. While early tests provided only few events which satisfied this relation later measurements with better temporal resolution provided many cases of thin magnetopause current layers which approximately satisfy the Walen relation [*Sonnerup et al.*, 1981; *Paschmann et al.*, 1986; *Gosling et al.*, 1990]. An additional test for the presence of a stationary magnetopause structure is the presence of a dHT frame [*Sonnerup et al.*, 1990]. Since the electric field is assumed constant there should be a reference frame in which the electric field is almost zero. An example which shows an excellent dHT frame but a poor Walen test is shown in Figure 7.15. The events typically are of short duration (few 10 seconds) indicating thin layers, show a mixture of magnetosheath and magnetospheric plasma, and a occur mostly for strong southward IMF.

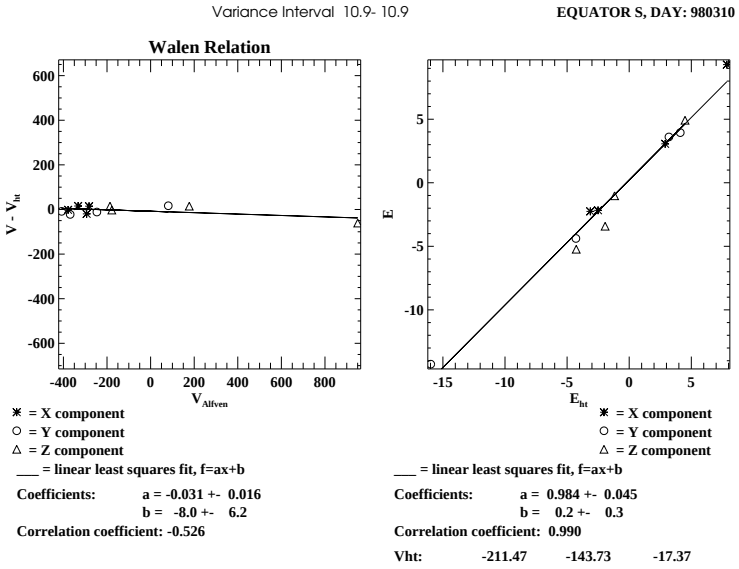

Figure 7.15: Tests of the dHT frame and the Walen relation for the data set shown before.

(b) The second class of events are so-called magnetic flux transfer events (FTE's) [*Haerendel et al.*, 1978; *Russel and Elphic*, 1978; *Paschmann et al.*, 1982; *Elphic*, 1990, 1995]. They show typically a strong bipolar variation of the magnetic field component normal to the magnetopause $\mathbf{B}_n$ together with a mixture of magnetosheath and magnetospheric electron populations. Various other typical properties are a correlation with southward IMF, an increase of total pressure and total magnetic field, a strong rotation of the field in the core of the event, and a good dHT frame. The typical duration is one to few minutes with a repetition rate of about 8 minutes. An example of FTE data is shown in Figure 7.16. The distribution of FTE's indicates the subsolar region as their source region. Furthermore typical amplitudes and scale sizes of FTE's require fast reconnection, i.e., with the Petschek reconnection rate.

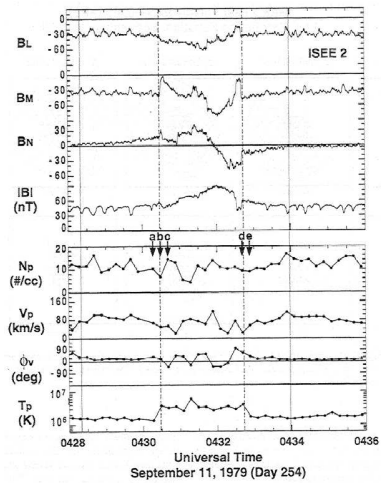

Figure 7.16: Example of FTE data after *Russel and Elphic* [1978].

7.3.6 Magnetopause Reconnection Models

The first explanation of FTE's was suggested by *Russel and Elphic* [1978] who assumed that patchy magnetic reconnection generates a magnetic flux tube or rope which connects the magnetospheric and magnetosheath sides and thus contains magnetosheath and magnetospheric particles. Magnetic field draped around this tube can generate the bipolar B_n signature as the flux tube moves along the magnetopause boundary as illustrated in Figure 7.17.

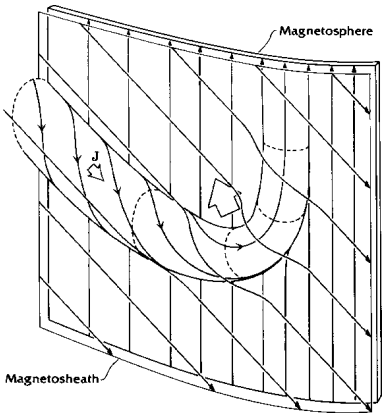

Figure 7.17: Sketch of a magnetic flux rope and the magnetic field draping from *Russel and Elphic* [1978].

There are various alternative models to explain FTE signature. The most basic possibility is a short duration reconnection pulse in a two-dimensional approximation [*Scholer*, 1988; *Southwood et al.*, 1988]. This process is illustrated as a result of a 2D MHD simulation in Figure 7.18. Here reconnection generates a plasma bulge which and the magnetic field around this bulge will generate a bipolar B_n signature.

Another model [*Lee and Fu*, 1985, 1986; *Lee*, 1995] employs reconnection at multiple x lines and the magnetic islands moving along the magnetopause will also cause a bipolar B_n signature. Both single x

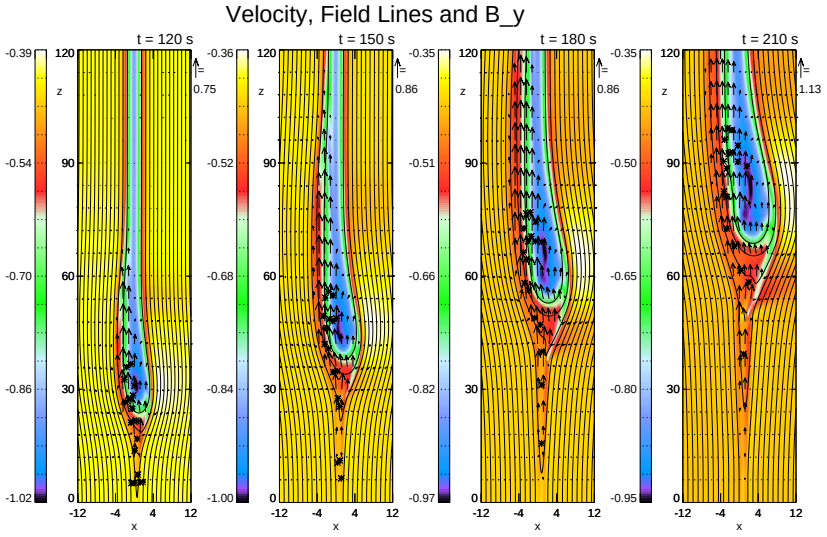

Figure 7.18: 2D simulation of localized reconnection.

line reconnection model and multiple x line reconnection have also been simulated in three-dimensional models, i.e., with a finite (small) length of the reconnection region [*Fu et al.*, 1990; *Otto*, 1990; *Schindler and Otto*, 1990; *Ma et al.*, 1994]. While the qualitative signatures are rather similar it appears that multiple x line reconnection and cases with relatively short x lines (3D) generate stronger and more realistic signatures. Currently it is unresolved whether reconnection occurs pulsed along a rather long x line along much of the dayside magnetopause or at multiple patches [*Nishida*, 1989; *Otto*, 1991, 1995] distributed of the subsolar region of the magnetopause as illustrated in Figure 7.19.

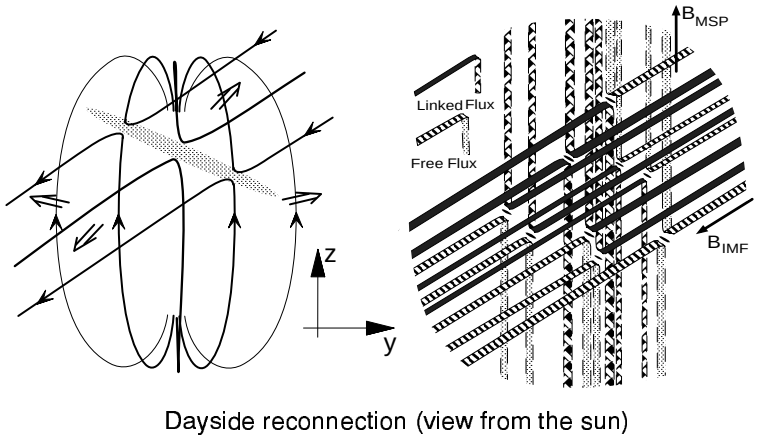

Figure 7.19: Sketch of reconnection in a single reconnection region (left) or at multiple small reconnection patches (right) in a view from the sun onto the dayside magnetopause.

Starting from very simple one-dimensional initial conditions, three-dimensional MHD simulations [*Otto*, 1999] demonstrate that reconnection initiated at a single reconnection site does not remains localized. Rather the initial single reconnection site decays into multiple reconnection sites which move along the current sheet.

Figure 7.20 shows the parallel electric field and the total pressure in the y, z plane at an early and a

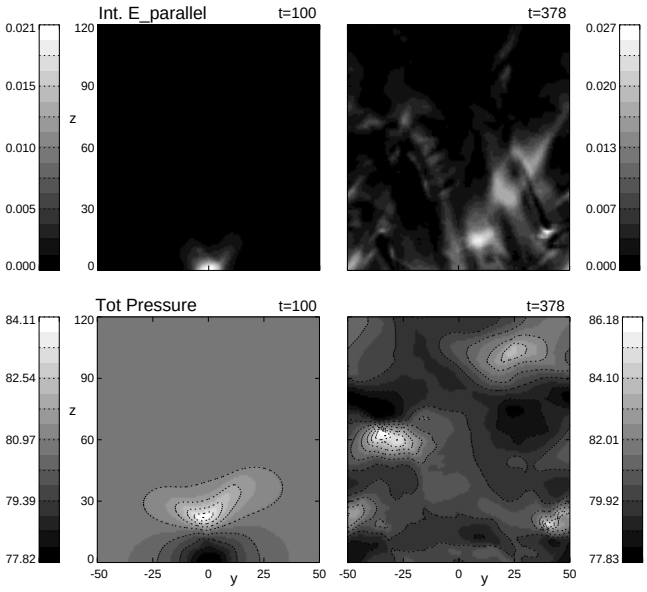

Figure 7.20: Parallel electric field distribution (top) and total pressure (bottom) from 3D MHD simulations of magnetic reconnection at an early (left) and a late (right) time of the simulations.

late time from a three-dimensional MHD simulation. Both quantities are integrated perpendicular to the current sheet (along x) to provide the global information which cannot be captures by a single cut through the 3D system. The parallel electric field is chosen because it represents the individual diffusion regions (reconnection sites) and maxima in the total pressure represent the locations with FTE-like properties. The initial configuration is a one-dimensional current sheet and reconnection is triggered only at single location. The figure demonstrates that reconnection is not confined to the initial onset location and FTE signatures develop in much of the simulation domain. The magnetic field configuration in Figure 7.21 shows two flux tubes elbow-like interlinked in the region of the total pressure maximum (time $t = 378$).

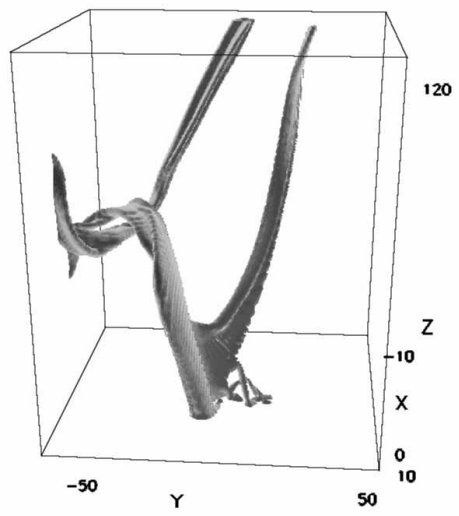

Figure 7.21: Example of magnetic flux ropes from a 3D MHD simulation.

7.4 Viscous Interaction

From the early days of magnetospheric physics it has been presumed that viscosity at the magnetospheric boundary may drive convection in the magnetosphere [*Axford and Hines*, 1961]. This is in particular evident from ionospheric convection. There is tailward convection in the polar cap at all times and only for strongly northward IMF two additional convection cells develop which show some sunward flow driven by high latitude (cusp) reconnection. This indicates that a portion of the magnetospheric convection is always driven by the magnetosheath flow and it is mostly accepted that about 10 to 20 kV of the polar cap potential (Figure 7.22) may be attributed to viscous processes at the magnetospheric boundary. In other words some of the tailward flow in particular close to the center of the convection cells may be on closed geomagnetic field lines.

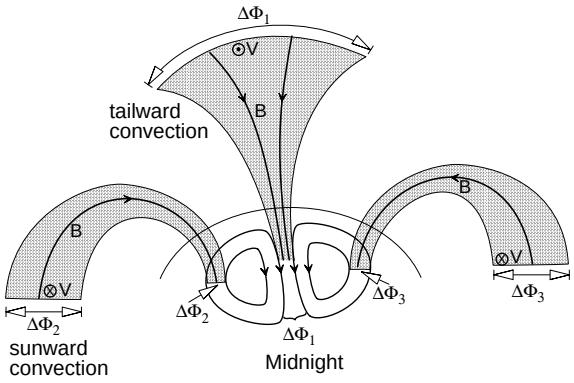

Figure 7.22: Sketch of ionospheric convection and cross polar cap potential.

In the outer magnetosphere the presence of the so-called low latitude boundary layer (LLBL, Figure 7.23) is indicative for viscosity driven convection. The LLBL consists of a mixture of magnetospheric and magnetosheath particles and plasma is flowing tailward although not quite as fast as in the adjacent magnetosheath. It is not yet clear whether the LLBL is entirely on closed field lines or is actually a mixture of closed and open magnetic field [*Newell and Meng*, 2003]. On the dayside boundary magnetic reconnection may generate this boundary layer. The average width of the LLBL increases away from the subsolar region to about 0.5 R_E close to the terminator. A diffusion coefficient of $D = 10^9\, m^2 s^{-1}$ is required [*Sonnerup*, 1980] to account for the LLBL quantitatively by mass and momentum diffusion .

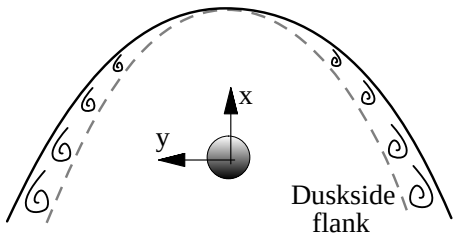

Figure 7.23: Sketch of the LLBL in the equatorial plane of the magnetosphere.

The presence of viscosity in a fluid implies that momentum can be transported in a direction transverse to the actual flow. However, as pointed out the magnetospheric plasma is highly collisionless meaning

there are no classical collisions of particles in most of the magnetosphere. This leaves two main physical mechanisms which may account for the viscous coupling.

Micro-instabilities: The magnetosphere has rather thin boundaries. These boundaries imply large gradients in many plasma properties such as density, temperature, or magnetic field. The free energy either directly due to the strong gradients or caused by electron/ion beams at the boundary can cause various instabilities. The effect of such instabilities is to relax the configuration which caused the instability which means to reduce the gradients or the fast relative motion of electrons and ions. Therefore they will cause diffusion of mass and momentum or friction similar to actual collisions of particles. Various micro-instabilities such as lower hybrid drift modes, ion acoustic modes, ion cyclotron, etc. have been suggested to account for viscous interaction [*La Belle and Treumann*, 1988; *Treumann and Baumjohann*, 1997]. However, while there are models to evaluate the resulting transport or diffusion coefficient, there are no self-consistent models of the full nonlinear coupling. This is an important point because of the rather large width of the LLBL close to the terminator.

Kelvin Helmholtz (KH) waves: An alternative mechanism for the formation of the LLBL is the Kelvin Helmholtz instability [*Chandrasekhar*, 1961]. This instability is present in many situations where two fluids stream relative to each other. Here the magnetosheath plasma (solar wind flow) moves fast relative to the plasma on the magnetospheric side which is almost at rest. Numerical simulations have demonstrated that the KH can in principle operate at the magnetospheric flanks [*Miura and Pritchett*, 1982; *Miura*, 1982] and it is able to transport energy and momentum from the magnetosheath into the magnetosphere [*Miura*, 1984]. However, there are two aspects worth considering.

The KH mode is stabilized by a variety of physical effects such as viscosity, surface tension, or a magnetic field aligned with the plasma flow. In the latter case the magnetic field is deformed by the plasma flow (Figure 7.24). This deformation requires additional energy such that the KH mode is stabilized [*Chandrasekhar*, 1961; *Chen et al.*, 1997; *Otto and Fairfield*, 2000]. In fact if the magnetic field energy density is higher than the energy in the shear flow the KH mode cannot operate at all.

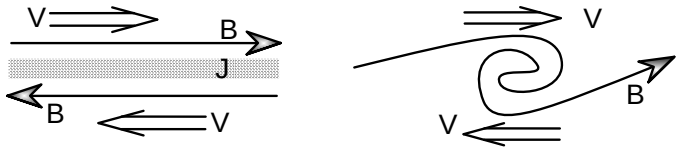

Figure 7.24: Sketch of KH evolution in the presence of a magnetic field.

Vice versa reconnection has rather similar properties. Magnetic reconnection is stabilized by shear flow (Figure 7.25). The reason for this is that the information velocity for magnetic reconnection is the Alfvén speed. Thus information that reconnection operates cannot propagate away from the x line if plasma flow is faster than the Alfvén speed such that reconnection cannot operate in the presence of fast plasma flow *Chen et al.* [1997]; *La Belle-Hamer et al.* [1995]. Therefore reconnection requires $\Delta V_A > \Delta v$ while the KH mode requires $\Delta v > V_{A,typ}$ along the k vector of the instability.

In the equatorial plane the geomagnetic field is strongly northward. Thus the KH instability can operate in the equatorial plane if the IMF is mostly northward or southward. Many observations show quasi-periodic signatures of density, velocity and magnetic field fluctuations [*Sckopke et al.*, 1981; *Chen and Kivelson*, 1993]. In a detailed study of such an event *Fairfield et al.* [2000] demonstrated that these

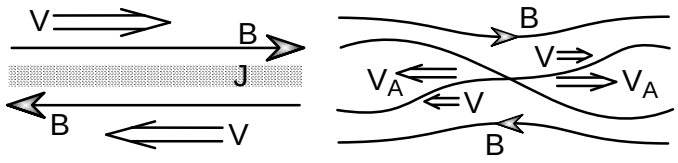

Figure 7.25: Sketch of magnetic reconnection in the presence of sheared plasma flow.

signature have a number of characteristic features (Figure 7.26). One of the most remarkable feature is the transient presence of negative B_z components although the geomagnetic and the interplanetary magnetic field were strongly northward.

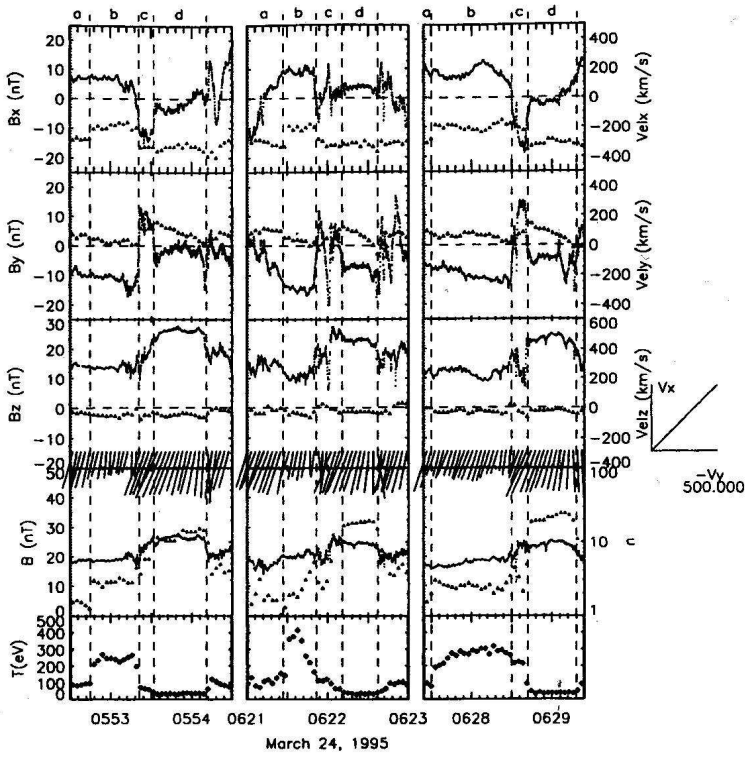

Figure 7.26: Three examples of quasi-periodic plasma and field signature from *Fairfield et al.* [2000].

In comparison two-dimensional MHD simulations (Figure 7.27) showed many of the same signatures and it was possible to identify individual signatures for instance for the entrance and exit of the SC into and out of the magnetosphere *Otto and Fairfield* [2000]. Particularly the twisting of the magnetic field in the KH vortex motion can generate negative B_z signature in small regions of space.

Simulation also demonstrated another important property of magnetic field deformation in the KH vortex. The KH mode is an ideal instability and therefore does not permit mass transport across the magnetospheric boundary. As argued before the initial field is usually strongly parallel such that reconnection cannot occur. However, the magnetic field deformation can generate strong local current sheets in the KH vortices (Figure 7.28). Thus reconnection is possible within these small scale current sheets *Otto and Fairfield* [2000].

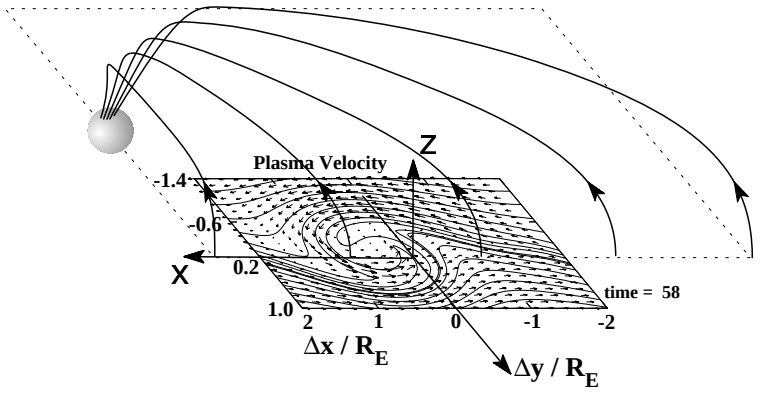

Figure 7.27: Geometry for 2D MHD simulations at the magnetospheric boundary.

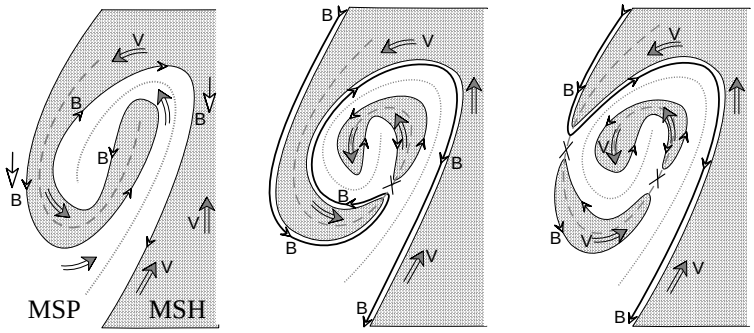

Figure 7.28: Schematic of the magnetic field deformation and subsequent reconnection inside KH vortices.

The mass transport into the magnetosphere for northward IMF is an unresolved problem. A possible mechanism for this transport is reconnection at high latitudes (above the northern cusp and below the southern cusp) which can connect IMF with the magnetosphere and thus capture magnetosheath material in the magnetosphere. An second plausible mechanism is reconnection inside KH vortices. In a quantitative evaluation of the reconnection inside of KH vortices (Figure 7.29) it is shown that the transport rate is indeed sufficient to explain an effective mass diffusion coefficient of $D = 10^9 m^2 s^{-1}$ [*Nykyri and Otto*, 2001].

It should be remarked that the KH mode may also occur at other locations on the magnetospheric boundary than discussed here. In fact for any orientation of the IMF there are always locations on the magnetospheric boundary where the magnetosheath and magnetospheric fields are approximately aligned.

Other processes at the magnetopause boundary Both magnetic reconnection and KH modes require an boundary that unstable with respect to either mode. However, energy and momentum can also be transferred by fluctuations carried by the solar wind or generated at the bow shock. It is suggested that solar wind pressure variations can also cause FTE signatures [*Sibeck*, 1990, 1992]. While pressure variations can cause some of these signatures it is not expected that the corresponding signature would have similar statistical properties such as a correlation to southward IMF.

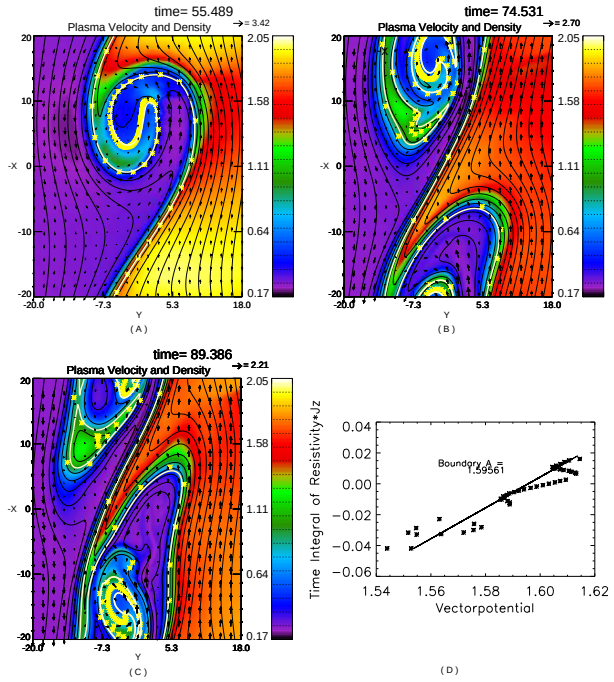

Figure 7.29: Results of magnetic reconnection inside of KH vortices from a 2D MHD simulation.

However, large increases in the solar wind velocity, density, or magnetic field have strong geomagnetic effects. They lead to a large scale compression of the magnetosphere and an intensification of all current systems. If a coronal mass ejection hits the magnetosphere the magnetopause can be pushed inside of 6 R_E which can for instance expose geostationary satellites to the solar wind.

It has also been suggested that plasma filaments with access momentum can actually penetrate the magnetopause and lead to a transport of mass into the magnetosphere [*Lemaire*, 1977]. This process has been termed impulsive penetration. Analytic and numerical simulations indicate that this may be possible if the magnetosheath and magnetospheric fields are highly aligned [*Schindler*, 1979a]. However, the actual capture of the filaments inside the magnetosphere would still require magnetic reconnection. Thus far there is no observational evidence of impulsive penetration.